Performance of a one-dimensional model of wave-driven nearshore alongshore tracer transport and decay

Elizabeth Brasseale[1], Falk Feddersen[1], Xiaodong Wu[2], and Sarah N. Giddings[1]

[1]Scripps Institution of Oceanography, 9500 Gilman Dr., La Jolla, CA 92093
[2]School of Oceanography, Shanghai Jiao Tong University, 1954 Huashan Rd., Shanghai 200030, China

Key Points:

- Dye (representing wastewater) in a 3D hydrodynamic model was reproduced using a fast and simple 1D wave-driven advection and loss model with significant skill
- Using a human illness probability threshold as a cutoff, the 1D model accurately predicted 3D model tracer concentration threshold exceedences in 89% of time steps
- 1D model forecast-informed daily beach advisories agreed with the 3D model on 9% more days than simulated weekly sampling

Corresponding author: Elizabeth Brasseale, `ebrasseale@ucsd.edu`

Abstract

In the San Diego-Tijuana region, current beach advisory metrics do not account for untreated wastewater flow into the ocean. Existing plume transport models are impractical for operational water quality forecasts because the relevant nearshore processes are poorly resolved. A 1D wave-driven advection and uniform loss model was developed for a 30 km nearshore domain spanning the border region. An along-shore uniform bathymetry is used, thus neglecting non-uniformities such as the inlet and shoal near the Tijuana River estuary (TJRE) mouth. Nearshore alongshore velocities were estimated using wave properties at an offshore location with the small angle, weak current approximation and a Rayleigh friction approximation. The 1D model was evaluated using the year-long hourly output of a 3D regional hydrodynamic model. Both velocity formulas had similar skill reproducing the alongshore-averaged nearshore alongshore velocities from the 3D model, but the 1D model run with the Rayleigh friction approximation had much lower skill in reproducing tracer. The 1D and 3D models agreed on tracer exceedance above a human illness probability threshold for 89% of time steps. Simulated daily beach advisories in the 3D model were compared with the 1D model and simulated weekly water quality sampling. 1D model-informed daily beach advisories agreed with the 3D model on 9% more days than simulated weekly sampling, and agreement did not decrease downstream of the TJRE inlet and shoal. This demonstrates that a 1D nearshore wave-advection model can reproduce nearshore tracer evolution from a 3D model over a range of wave conditions ignoring bathymetric non-uniformities.

Plain Language Summary

In the San Diego-Tijuana region, water quality problems originating from inadequate wastewater treatment are not well predicted by rainfall or weekly water sampling. A 1D model of the nearshore ocean was developed to predict how dye (standing in for wastewater) is moved along the coastline by wave-driven currents. The 1D model uses a straight 30 km shoreline, neglecting complex bathymetry such as that near the mouth of the Tijuana River estuary (TJRE). The 1D model was compared to a complex 3D regional ocean model. First, it was shown that nearshore currents could be accurately calculated using an offshore wave buoy. Using only wave-driven currents, the 1D model could accurately reproduce the dye patterns seen in the 3D model in a fraction of the time. The 1D model predicted daily beach advisory conditions on 87% of the same days as the 3D model, which was a 9% improvement over simulated weekly water sampling. Depending on the analysis, the 1D model performance decreased only slightly or not at all downstream of the TJRE. Therefore, a simple, fast, 1D model with a uniform coastline can

be used in place of or in concert with complex 3D models in applications where 3D models are impractical, such as public health websites.

1 Introduction

When nearshore waters are contaminated with pollution, surfers and swimmers can ingest waterborne pathogens that cause gastrointestinal illness (Shuval, 2003). Nearshore pollution reduces tourism, as beaches are issued advisories or closures when waterborne pathogens are detected. Water pollution can originate from non-point sources, such as urban and agricultural run-off after rain, or from point sources, such as wastewater infrastructure failure (de Brauwere et al., 2014). The San Antonios de los Buenos Wastewater Treatment Plant (SABWTP) is an example of a point source of untreated sewage in the San Diego-Tijuana region. Of the 50 million gallons per day (mgd) outflow from SABWTP, treatment capacity is only 15 mgd and the remaining 35 mgd are untreated (ARCADIS, 2019). The SABWTP outfall flows directly onto the beach near Punta Bandera (PB), 10 km south of the United States-Mexico border. On a straight coastline, pollution point sources along the beach can contaminate nearshore waters tens of kilometers away because tracers are transported along coast effectively and exported offshore slowly (Grant et al., 2005; Hally-Rosendahl et al., 2015; Feddersen et al., 2016; Grimes et al., 2021). The coastline of the San Diego bight has over thirty kilometers of mostly straight, sandy beach with bathymetric irregularities only near the Tijuana River Estuary (TJRE) and coastline curvature at the northern end of the bight near the San Diego Bay entrance (Fig. 1).

In San Diego county, beach advisories are issued when fecal indicator bacteria (FIB) are found in weekly beach water quality sampling or after rainfall (San Diego County, n. d.). However, beach advisory postings based on weekly testing have been estimated to be inaccurate up to 40% of the time because FIB concentrations can change quickly and are spatially heterogeneous (J. Kim & Grant, 2004). Further, testing for FIB may not be a sufficient indicator of the likelihood of illness for beach goers (Boehm et al., 2009). FIB decay faster than other pathogens that live in wastewater and cause illness in swimmers, such as human norovirus (Boehm & Soller, 2020). Norovirus is a leading cause of gastrointestinal disease among wastewater pathogens and is plentiful in raw sewage (Boehm & Soller, 2020). Rainfall is also an incomplete indicator. Rainfall is commonly used in the United States to indicate water quality because stormwater runoff from cities and farms is high in FIB from either human or animal sources, or both (Francy, 2009; Stidson et al., 2011; Aguilera et al., 2019). In the San Diego-Tijuana region, rainfall causes additional water quality problems because the South Bay International Wastewater Treatment Plant closes during rain events and diverts flow to the TJRE to preempt infrastructure clogging (ARCADIS, 2019). However, rainfall does not account for dry weather runoff, which is increasingly recognized to have a disproportionate effect on water quality at urban coastlines (Rippy et al., 2014). Inadequacy of wastewater treatment plant infrastructure, as is the case for SABWTP, is a large source of dry weather runoff. Microbial source testing during dry weather has found evidence of the SABWTP wastewater plume on the shoreline 20 km north of PB (Zimmer-Faust et al., 2021). Coupled hydrodynamic and human illness models suggest SABWTP is responsible for exposing more beachgoers to wastewater than the rainfall-dependent TJRE (Feddersen et al., 2021). To capture SABWTP pollution, current beach advisory criteria should be supplemented with dynamical modeling.

Some models of wastewater plume transport in the San Diego-Tijuana region do currently exist, but have drawbacks. A plume tracker model advects particles released from the TJRE mouth, PB, and the South Bay ocean outfall using high-frequency radar (HFR) currents to make daily water quality predictions (S. Y. Kim et al., 2009). The shoreline exposure to FIB in the plume tracker model captured 70% of beach advisories from water quality sampling during rain events over four years (S. Y. Kim et al., 2009). However, the plume tracker has several issues (e.g., Rogowski et al., 2015). First, pollution plumes are often located within 1 km of shore (Wu et al., 2020; Grimes et al., 2021) where HFR cannot estimate currents. In addition the data coverage on the shelf varies spatially and temporally and the uncertainties in the estimated currents are up to 10 $\mathrm{cm\,s^{-1}}$. Lastly, the plume tracker particles are surface trapped and thus dilution due to vertical mixing is neglected. Currents in the nearshore region are predominately driven by wave breaking (Feddersen, 1998; Lentz et al., 1999), and are uncoupled from inner shelf currents. A hydrodynamic model of the San Diego-Tijuana coastal ocean that resolves both the shelf and the nearshore and tracks plumes from both TJRE and PB (referred to as the "SD Bight model") was built by coupling an ocean model to a wave model using the COAWST framework (Wu et al., 2020; Feddersen et al., 2021) (described in Section 2.1). However, the SD Bight model is computationally expensive and currently only exists as a hindcast.

An alternative solution is a model of only the nearshore. Transport through the nearshore is dynamically simple. Alongshore momentum is dominated by wave-breaking which can be estimated from an offshore wave buoy (Feddersen, 1998; Lentz et al., 1999). A nearshore model is appropriate to the problem because the input (SABWTP outflow), dynamics (wave-driven advection), and desired output (shoreline exposure) are all located nearshore. Previous nearshore wave-advection models have reduced the problem to a 1D alongshore-uniform grid by cross section-averaging tracer concentrations and alongshore transport (Boehm, 2003; Boehm et al., 2005; Grant et al., 2005; Grimes et al., 2021). The effects of pathogen mortality and offshore transport can be represented by loss of dye from the 1D domain (Boehm, 2003). Operationally, such a model would be orders of magnitude faster than a full hydrodynamic regional model, and therefore more practical for daily forecasts and ensemble studies. However, validation of 1D nearshore models has been limited by the available observational data. Historical water quality records may span decades, but the samples are only taken once per week. This sampling rate is too infrequent to capture the propagation of individual plumes along the shoreline. Models tuned to historic water quality data such as Boehm (2003) have demonstrated ensemble agreement, but cannot demonstrate the reproduction of individual events. Field experiments can observe the propagation of individual plumes at high spatial and temporal resolution, but only span short time periods, for example, 5 hr (Rippy et al., 2013), 24 hr (Grant et al., 2005), or 30 hr (Grimes et al., 2021). Models validated by field studies can reproduce individual plume events well (Grimes et al., 2021), but do not demonstrate model performance under a range of wave conditions. Here, we will evaluate performance of a 1D wave-advection model in reproducing individual plume events over different seasons using the SD Bight model, which has hourly output for a year.

The 1D model assumes that wave-driven alongshore advection in the nearshore can be calculated from wave properties at an offshore location. On a long, straight coastline, the alongshore momentum balance in the nearshore is dominated by bottom stress and the cross-shore gradient of the forcing from breaking waves (Longuet-Higgins, 1970; Feddersen, 1998; Ruessink et al., 2001),

$$\tau_{b,y} = -\frac{\partial S_{xy}}{\partial x}, \tag{1}$$

where $\tau_{b,y}$ is the bottom stress in the alongshore direction, S_{xy} is the off-diagonal component of the radiation stress, y is the alongshore coordinate, and x is the cross-shore coordinate. Because wave energy is conserved until breaking, the wave properties relevant for S_{xy} can be estimated from properties at an offshore wave buoy (details in Section 2.4). The alongshore current (averaged over several wave periods), v, can be found by relating v to the bottom stress, $\tau_{b,y}$,

$$\tau_{b,y} = \rho C_D \langle |\vec{u}| v \rangle, \tag{2}$$

where ρ is the density of seawater, $\vec{u}$ is full velocity vector, C_D is a dimensionless drag coefficient, and $\langle \cdot \rangle$ is a time average. Two approximations can be made to calculate $\langle |\vec{u}| v \rangle$ in the nearshore. The first is the weak current approximation, which holds when the current is weaker than the wave orbital velocities, $v < \sigma_{\vec{u}}$, where $\sigma_{\vec{u}}$ is the total velocity variance, $\sigma_{\vec{u}}^2 = \sigma_u^2 + \sigma_v^2$. The second is the small angle approximation, which holds when the wave propagation direction is near shorenormal, $\sigma_v < v$. Using the small angle and weak current approximations, the bottom stress can be represented (Wright & Thompson, 1983),

$$\tau_{b,y} = 1.5\sqrt{\frac{\pi}{2}}\rho C_D \sigma_{\vec{u}} v. \tag{3}$$

Some studies have further approximated bottom stress by assuming a constant $\sigma_{\vec{u}}$, also known as a linear or Rayleigh friction approximation (Lentz et al., 1999; Feddersen et al., 2000; Grimes et al., 2021),

$$\tau_{b,y} = \rho\mu v, \tag{4}$$

where μ is a constant with dimensions m s^{-1}. Using wave-estimated alongshore currents, the nearshore transport of a tracer (such as untreated wastewater) can be modeled. This study will compare model skill of 1D models run with alongshore velocities estimated using (3) and (4).

A potential challenge that has not been addressed in previous nearshore transport models is the effect of alongshore-variable bathymetry on alongshore transport. Along the San Diego-Tijuana shoreline, the TJRE mouth lies between PB and many of the recreational beaches known to be affected by wastewater from the SABWTP (Fig. 1). During times when the Tijuana River is flowing, the impact of the TJRE plume on the alongshore transport of the wastewater from PB is unknown. Larger buoyant plumes have been demonstrated to form a barrier to alongshore transport (Banas et al., 2009). Even though the Tijuana River only flows episodically, the estuary mouth is a permanent topographic feature that may affect the alongshore transport of untreated wastewater from PB. Tidal currents through the estuary mouth may affect alongshore transport through wave-current interaction, offshore ejection or by retaining dye in the estuary, a process known as tidal trapping. The effect of tidal trapping on alongshore transport is not known, but in estuarine channels, tidal trapping has been found to disperse the along-estuary distribution of salt (Okubo, 1973; MacVean & Stacey, 2011). It is hypothesized, then, that over many tidal cycles, tidal trapping of a tracer in the TJRE would disperse the tracer concentrations along the shoreline. Another hypothesized effect of the TJRE would be the local acceleration of wave-driven transport over the shoal built of sediment deposited outside the estuary mouth. While this analysis cannot tease out each of these potential mechanisms (i.e., buoyant plume, wave-current interactions, offshore ejection, tidal trapping, non-uniform bathymetry), to examine the net effect of the TJRE in this analysis, model skill will be compared upstream (south) and downstream (north) of the TJRE.

In summary, the goal of this study is to use the SD Bight model, with hourly nearshore current and tracer concentration data from December 12, 2016 to December 20, 2017 to evaluate the skill of a 1D nearshore transport model. The region of interest is a 30 km stretch of coastline from the SABWTP outflow at PB to Hotel del Coronado (HdC) (Fig. 1). Comparison with a realistic 3D hydrodynamic model will demonstrate how well regional nearshore transport can be modeled neglecting inner shelf circulation and using wave properties at a single offshore source using (3) and (4). By doing this, we hope to address the following questions:

1. Can nearshore alongshore transport be well-represented using uniform nearshore alongshore velocity estimated from an offshore location (such as from a wave buoy), and is a linear bottom stress approximation (4) sufficient for estimating alongshore velocity?
2. Can alongshore tracer distributions be adequately reproduced in a nearshore model which neglects shelf circulation?
3. How does alongshore-variable bathymetry (i.e., the presence of an estuary inlet and shoal at the TJRE mouth) impact nearshore model skill?

The drawbacks of existing dynamic models, including lack of resolution of relevant processes (S. Y. Kim et al., 2009), computational expense (Wu et al., 2020), and lack of calibration across different hydrodynamic conditions (Grimes et al., 2021), are well-documented obstacles to the implementation of dynamic models for real-time water quality prediction (Elko et al., 2022). The 1D model developed here offers a solution to these challenges. While we are testing this 1D model in a particular region with known water quality problems, we expect the results to be applicable broadly to the skill of 1D wave-advection models for the transport of other tracers (e.g. sediment, plankton, or microplastics) and other coastlines.

2 Methods

2.1 3D realistic SD Bight model

The SD Bight model grid covers a 30 km stretch of coastline from 32.45 N (south of PB) to 32.75 (around Point Loma) and extends 10 km offshore (Fig. 1b). This SD Bight model has been used in other recent studies investigating the transport of tracers across the surf zone and inner shelf in the San Diego-Tijuana region (Wu et al., 2020, 2021a,b,c; Feddersen et al., 2021). The model uses the COAWST (Coupled-Ocean-Atmosphere-Wave-Sediment-Transport) modeling system (Kumar et al., 2012; Warner et al., 2010). The SD Bight model couples Regional Ocean Modeling Systems (ROMS), a 3D hydrostatic ocean model with terrain-following vertical coordinates (Shchepetkin & McWilliams, 2005), with Simulating WAves Nearshore (SWAN), a spectral wave model (Booij et al., 1999).

The resulting model resolves surf zone, estuarine, and shelf dynamics. The SD Bight model uses realistic atmospheric forcing (e.g. wind, heating, atmospheric pressure) from NOAA/NAM, tides, and river flow from the Tijuana, Otay, and Sweetwater rivers. The oceanic boundary conditions (temperature, salinity, sea surface height, and currents) are generated by a series of three one-way-nested parent grids (Wu et al., 2020). There are 10 vertical levels. The horizontal grid is rectangular and telescopic, such that the horizontal resolution is highest in the surf zone near the TJRE mouth (8 m) and lower offshore over the shelf (110 m). The SD Bight model hindcast simulation used here runs from December 12, 2016 to December 20, 2017. The baroclinic computational time step varied from one to two seconds and the wave field was updated every four minutes. SWAN and ROMS exchanged wave field and ocean condition information every 12 minutes. Model output was saved hourly to resolve tides. This SD Bight model hindcast included a dye tracer to simulate the evolution of an untreated wastewater plume (Fig. 1c). The dye tracer was input to the model at PB, the location of the SABWTP outfall, at a concentration of 0.7 to match the treatment of 15 mgd of the total 50 mgd outflow (ARCADIS, 2019). Complete details of the model implementation are in Wu et al. (2020).

Here, we define the nearshore as the region from the 5-m isobath (contoured in Fig. 1) to the shoreline, a definition which spans the surf zone and a portion of the inner shelf. The 5-m isobath was chosen because it is the furthest offshore extent of the surf zone for range of wave heights observed during the simulation period. This is the region typically used by surfers and swimmers who could be harmed by exposure to sewage. The location of the 5-m isobath is found for every time step to capture tidal variation. Average dye concentrations and alongshore transport in the nearshore region were extracted from the SD Bight model from PB to the beach at HdC (red line in Fig. 1b). Alongshore distance from PB, y, was calculated following the shoreline, defined such that positive y is to the right when facing the sea (roughly north). Dye and velocity were averaged vertically and in the cross-shore direction within the nearshore region. Velocity vectors were then rotated from grid coordinates into local alongshore and cross-shore coordinates using shorenormal angles estimated from the model grid. These shorenormal angles were consistent with current principal axes. SD Bight model alongshore velocity was then alongshore averaged from PB to HdC to get a representative year-long time series, $\bar{v}_{\mathrm{C}}(t)$. Alongshore-varying nearshore alongshore velocity and dye extracted from the SD Bight model will be referred to as $v_C(t, y)$ and $C_{\mathrm{C}}(t, y)$ respectively.

Figure 1. a) Regional map with study area indicated (star) along United States-Mexico border (dotted line). b) SD Bight model domain with annotated landmarks. Color indicates bathymetry. The red line highlights the 29 km stretch of coastline represented in the 1D model. Magenta triangle indicates the source of wastewater to the surf zone at Punta Bandera (PB). Yellow circles represent popular recreational beaches: Playas Tijuana (PTJ), Imperial Beach (IB), Silver Strand Beach (SS), and Hotel del Coronado (HdC). Blue diamond is location of CDIP Imperial Beach nearshore wave buoy. The green triangle indicates the head of the Tijuana River estuary (TJRE). c) Snapshot of surface dye concentrations on a logarithmic scale on July 11, 2017 12:00:00 when a plume from PB was transported up the coast during a long-duration south swell. Model bathymetry contoured in b) and c) at 5, 10, and 20m isobaths.

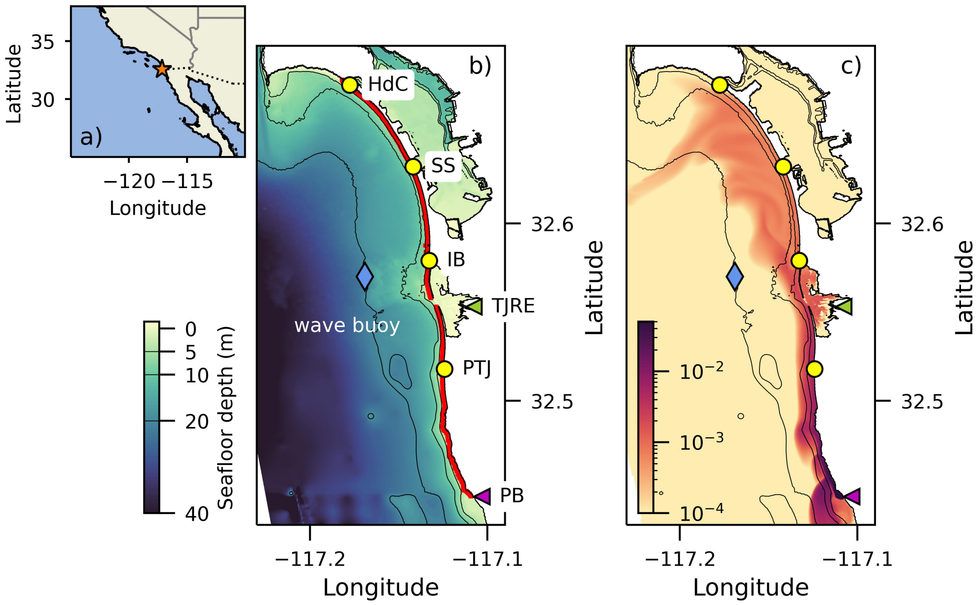

2.2 Nearshore 1D tracer advection/loss model

Here we describe our 1D tracer advection/loss model for a nearshore dye tracer transported alongshore by wave-driven currents with loss due to physical (i.e., offshore export of dye from the nearshore region) and biological (i.e., pathogen die off) processes. Similar 1D models of dye evolution have been used in studies that consider the transport of waterborne pathogens along beaches (Boehm, 2003; Boehm et al., 2005), in lagoons (Steets & Holden, 2003), and in streams (Jamieson et al., 2005; Cho et al., 2010), although the source of advection differs to fit the appropriate drivers of ambient currents in those environments. This model is hereafter referred to as the 1D model. The 1D model solves,

$$\frac{\partial C_{1\mathrm{D}}(t,y)}{\partial t} = -v_{1\mathrm{D}}(t)\frac{\partial C_{1\mathrm{D}}(t,y)}{\partial y} - (k_B + k_P)C_{1\mathrm{D}}(t,y), \tag{5}$$

where y is the alongshore coordinate, t is time, $C_{1\mathrm{D}}$ is the dye concentration, $v_{1\mathrm{D}}$ is the wave-driven alongshore current, and k_P and k_B are constant loss terms parameterizing physical and biological processes that reduce nearshore dye concentrations, respectively.

Both $v_{1\mathrm{D}}$ and loss terms (k_P and k_B) are assumed alongshore-uniform and effects of shoreline curvature are neglected.

The first loss parameter, k_B, represents the inverse timescale of pathogen die-off. The 1D model used a 10-day e-folding time scale, $k_B = 1.6 \times 10^{-6}\mathrm{s}^{-1}$, to match the prescribed dye behavior in the SD Bight model (Wu et al., 2020; Feddersen et al., 2021). The 10-day timescale used in the SD Bight model corresponds to the mortality of norovirus (Boehm et al., 2018). The estimated mean e-folding time scales for other common wastewater pathogens in seawater range from less than one day (for *Campylobacter*) to one month or more (for *Giardia*) (Boehm et al., 2018).

The second linear loss parameter k_P represents the cross-shelf tracer exchange between the nearshore region and the inner shelf. The k_P parameter may be thought of as an exchange velocity, u_{ex}, divided by the cross shore distance from the shoreline to boundary between the nearshore and the shelf, L (Hally-Rosendahl et al., 2014; Grimes et al., 2021). This cross-shelf exchange is often driven by rip currents in observations (Hally-Rosendahl et al., 2014, 2015; Moulton et al., 2017, 2021) and models (Hally-Rosendahl et al., 2014; Suanda & Feddersen, 2015; Kumar & Feddersen, 2017). Studies in the surf zone have found that exchange between the surf zone and inner shelf produces a net non-zero offshore dye flux (Hally-Rosendahl et al., 2014; Grimes et al., 2021), which can be parameterized as a monotonic decay of nearshore dye concentration.

Dye was added to the 1D model using a Dirichlet boundary condition, constant C_0 at y=0 km. This boundary condition represents the mean dye concentration adjacent to the PB outfall considering a persistent flux of 0.7 dye water that dilutes upon entering the ocean and is not completely retained in the nearshore. Small plumes partially escape being trapped by waves in the nearshore when waves are weak or the tide is high (Rodriguez et al., 2018; Kastner et al., 2019). Model output will be compared for $y >$ 2 km because rapid diffusion occurs near the dye source in the SD Bight model which is not represented in the 1D model. The tracer evolution equation (5) was solved numerically for $C_{1\mathrm{D}}(y, t)$ with a first-order upwind advection scheme, which is simple and unconditionally stable (Roe, 1986). The 1D model used a time step, $\Delta t = 18$ s and a grid cell size $\Delta y = 32.85$ m. Alongshore diffusivity was neglected (see discussion in Section 4.2).

2.3 Determining dye parameters k_P and C_0

A value for k_P was used for all 1D model runs based on dye concentrations from the SD Bight model, and C_0 was tuned using an iterative search optimization method to maximize model performance for each 1D model run. The physical rate of dye loss was determined from $k_P = k - k_B$, where k is the total rate of dye loss from the nearshore region of the SD Bight model. The rate of dye loss was estimated beginning with the exponential decrease in the time-averaged nearshore dye concentrations, $\langle C_\mathrm{C} \rangle$, with y. The rate of spatial decay is converted into a temporal decay rate using a velocity scale, V (RMS of v_C),

$$k = V \frac{d \ln \langle C_\mathrm{C} \rangle}{dy}. \tag{6}$$

The optimal choice for each C_0 varied based on the value of k_P (and vice versa) and the velocity model. Alternative parameter selection methods were considered, including fixing both parameters to estimates from the SD Bight model or a multivariate optimization that iteratively tuned both parameters. Fixing one parameter and tuning the other was opted for as a hybrid approach. With the hybrid approach, C_0 was chosen as the tuning parameter because the mean value of dye near PB in the SD Bight model was sensitive to the location at which it was estimated, and k_P had precedence in literature available for comparison. Resulting k_P using equation (6) and optimized values for C_0 are listed in Section 3.2.

2.4 Calculating velocity from wave properties

The 1D model alongshore-uniform wave-driven nearshore alongshore velocity, $v_{1\mathrm{D}}(t)$, was estimated from wave properties at an offshore location (32.56957 N, -117.1688 E, 20-m isobath, Fig. 1), the position of the Imperial Beach Nearshore Buoy operated by the Coastal Data Information Program (CDIP). To make use of the established relationship between surf zone alongshore currents and waves, (1) (Longuet-Higgins, 1970; Feddersen, 1998; Ruessink et al., 2001), the alongshore currents in the nearshore region are presumed to be proportional to surf zone alongshore-mean alongshore currents.

To estimate $v_{1\mathrm{D}}$, first the right hand side of (1) was simplified using a finite difference approximation. Radiation stress begins decreasing in the surf zone where waves break, and S_{xy} decreases to zero at the shoreline. To average this wave forcing across the nearshore domain, the change in S_{xy} to zero is divided by the cross-shore distance to the 5-m isobath L,

$$\frac{\partial S_{xy}}{\partial x} \approx \frac{S_{xy}(t)}{L}. \tag{7}$$

For simplicity and generalizabilty to locations without well-known bathymetry, (7) was evaluated with a constant L, set to the mean of the tidally-varying distance to the 5-m isobath. A narrow-banded representation of S_{xy} is used (Longuet-Higgins, 1970),

$$S_{xy}(t) = E(t) \frac{c_g(t)}{c_p(t)} \cos\theta'(t) \sin\theta'(t), \tag{8}$$

where E is the wave energy, c_g is the group velocity, c_p is the phase velocity, and θ' is the difference between the mean wave direction, θ, from shorenormal, θ_{SN}. For these estimates of alongshore-uniform wave-driven alongshore velocity, θ_{SN} was a constant chosen to optimize model performance. The wave energy term in (8), E, was determined using,

$$E(t) = \frac{1}{16}\rho g H_s(t)^2, \tag{9}$$

where g is gravitational acceleration, ρ is the mean seawater density, and H_s is the significant wave height.

We evaluated two bottom stress formulas, (3) and (4), resulting in two alongshore current estimates. The total velocity variance $\sigma_{\vec{u}}$ in (3) can be written out as a function of H_s at the 5-m isobath. By definition, $H_s = 4\sigma_\eta$, where the σ_η is the standard deviation of the sea surface height (Young, 1999). Because velocity and sea surface height have the same frequency, $\sigma_{\vec{u}}$ is proportional to σ_η, using a scale factor of $\sqrt{\frac{g}{h}}$ to change the dimension (Mei, 1989). The resulting expression for $\sigma_{\vec{u}}$ is,

$$\sigma_{\vec{u}}(t) = \sqrt{\frac{g}{h_{5\mathrm{m}}}}\frac{H_{s,5\mathrm{m}}(t)}{4}, \tag{10}$$

where h is the constant depth of the water column. $H_{s,5\mathrm{m}}$ can be estimated from the significant wave height at the offshore location of the wave buoy, $H_{s,\mathrm{WB}}$ using Snell's Law and the conservation of wave energy flux given the difference in water depths. For this data set, $H_{s,5\mathrm{m}} = 0.88H_{s,\mathrm{WB}}$ on average. Combining (1), (3), (7), and (10) gives the following equation for $v_{1\mathrm{D}}$,

$$v_{1\mathrm{D}}(t) = -\frac{8}{3L\rho C_{\mathrm{D}}}\sqrt{\frac{2h_{5\mathrm{m}}}{\pi g}}\frac{S_{xy}(t)}{H_{s,5\mathrm{m}}(t)}, \tag{11}$$

where C_{D} has flexibility as a fitting parameter. The velocity calculated using the Rayleigh friction model will be called $v_{1\mathrm{DR}}$. In the Rayleigh friction velocity model, (4), $\sigma_{\vec{u}}$ is constant. Constant $\sigma_{\vec{u}}$ and combining (1), (4), and (7), gives the following formula for $v_{1\mathrm{DR}}$,

$$v_{1\mathrm{DR}}(t) = \frac{S_{xy}(t)}{\rho\mu L}. \tag{12}$$

Values for C_D and μ, for $v_{1\mathrm{D}}$ (11) and $v_{1\mathrm{DR}}$ (12) respectively, were calculated using a simple linear regression (with intercept fixed to zero) between the wave-estimated velocity and $\bar{v}_{\mathrm{C}}$.

1D model performance will depend on the accuracy of the velocity formulas as well as on model assumptions such as using a uniform grid which neglects shoreline curvature and a uniform dye loss parameterization which neglects inner shelf circulation. To test the assumptions of the 1D model method not related to the advection calculation, (5) was also solved with the alongshore-varying nearshore alongshore velocity extracted from the SD Bight model, $v_{\mathrm{C}}(t, y)$. "1DC model" will refer to the run using $v_{\mathrm{C}}(t, y)$ with dye output C_{1DC}. "1D model" will refer to the model run using $v_{\mathrm{1D}}(t)$ (i.e., the small angle, weak current approximation, (11)) with dye output C_{1D}. "1DR model" will refer to the model run using v_{1DR} (i.e., the Rayleigh friction model, (12)) with dye output C_{1DR}. The 1D grid resolution, time step, and dye loss parameter (k_P and k_B) were the same for all three runs, but the 1DC run used a modified numerical implementation that allowed for alongshore-varying alongshore advection. Although the numerical implementation is modified to allow for alongshore velocity variations, the 1DC model can be viewed as an upper-bound on 1D model performance with these assumptions (fixed L, uniform dye loss parameters k_B and k_P, etc.).

2.5 Performance metrics

Performance for the 1D models was evaluated by comparing C_{1D}, C_{1DR}, and C_{1DC} with C_{C}, the nearshore dye extracted from the SD Bight model. Three performance metrics were used: Pearson's correlation coefficient (R), the normalized root-mean-square-error (NRMSE), and Willmott's skill score (WSS). To calculate NRMSE, the root-mean-square-error was normalized by the time-averaged value of C_{C} for each alongshore location. WSS is a comprehensive model agreement metric that scales the mean square error by the potential error for a data set (Willmott, 1981),

$$\mathrm{WSS} = 1 - \frac{\Sigma_{i=1}^{i=N}(m_i - o_i)^2}{\Sigma_{i=1}^{i=N}(|m_i - \langle o \rangle| + |o_i - \langle o \rangle|)^2} \tag{13}$$

where m is the 1D model value, o is the SD Bight model value, and N is the number of data points. The range of WSS is 0 to 1, with 1 being best. The range of R is -1 to 1, with 1 being best. The NRMSE is positive definite, with 0 being best. When describing trends in the metrics together, "better" means an increase in WSS and R and a decrease in NMRSE.

The condition $C_{\mathrm{BAC}} = 5\times10^{-4}$ was chosen as a cut off value to determine whether dye plume events were significant, referred to as the beach advisory condition. This C_{BAC} corresponds to a 10% likelihood of swimmer illness (Feddersen et al., 2021). When dye concentrations exceed C_{BAC}, norovirus concentrations in the wastewater plume would be sufficient to require posting a beach advisory by EPA standards (U.S. Environmental Protection Agency, 2014).

3 Results

3.1 Nearshore current calibration, drag coefficients, and shorenormal

Both $v_{1\mathrm{D}}$ and $v_{1\mathrm{DR}}$ were calibrated by fitting C_d and μ using a linear regression with $\bar{v}_{\mathrm{C}}$ to a slope of 1 with no intercept (Fig. 2d, e). The resulting $v_{1\mathrm{D}}$ and $v_{1\mathrm{DR}}$ had strong agreement (R$>$ 0.8) with $\bar{v}_{\mathrm{C}}$ (Fig. 2). The small angle, weak current drag coefficient was fit to $C_{\mathrm{D}} = 0.004$, consistent with the value of 0.0033 found for the surf zone in Feddersen (1998). The Rayleigh friction coefficient was fit to $\mu = 3.9\times10^{-3}$ m s^{-1}, consistent with Rayleigh friction coefficient values of 5×10^{-3} in Lentz et al. (1999) and 2.5×10^{-3} in Grimes et al. (2021). The resulting wave-driven nearshore alongshore velocities captured the variations in the nearshore alongshore velocities from the SD Bight model (Fig. 2b, c). The Rayleigh friction model $v_{1\mathrm{DR}}$ overestimated $\bar{v}_{\mathrm{C}}$ when $|\bar{v}_{\mathrm{C}}| > 20$ cm s^{-1} and underestimated small $\bar{v}_{\mathrm{C}}$ during summertime (Fig. 2c, e). This is consistent with previous evaluations of Rayleigh friction which works poorly across a large range of v (Feddersen et al., 2000). Both $v_{1\mathrm{D}}$ and $v_{1\mathrm{DR}}$ overestimated $\bar{v}_{\mathrm{C}}$ during the biggest southerly waves in winter (spikes between Jan 1 and Mar 1 in Fig. 2b, c).

The 1D model was sensitive to the choice of θ_{SN} because wave direction is often near shorenormal, and the sign of θ' determines the direction of the velocity. Over the stretch of shoreline of interest, the mean shorenormal angle is 260°, varying from 240° to 270°. Shorenormal angles are closest to 270° in center and decrease towards the domain edges. Using uniform shorenormal angle $\theta_{\mathrm{SN}} = 263°$ resulted in best R, NRMSE, and WSS of $v_{1\mathrm{D}}$ out of one hundred θ_{SN} values tested in the range 240° to 270°. Overall, $v_{1\mathrm{D}}$ performed better than $v_{1\mathrm{DR}}$ using all skill metrics. The SD Bight model alongshore-varying nearshore alongshore velocities $v_C(t, y)$ used in the 1DC model and to derive $\bar{v}_{\mathrm{C}}(t)$ were locally rotated using alongshore-varying shorenormal angles estimated from the land mask in the grid (described in Section 2.1).

3.2 Dye parameter calibration, k_P and C_0

Beginning 5 km north of PB, $\langle C_{\mathrm{C}}\rangle$ decays exponentially with y at an e-folding length scale of 7.9 km (Fig. 3). A velocity scale $V = 0.1$ m s^{-1}, the RMS of $\bar{v}_{\mathrm{C}}$ from the SD Bight model (Fig. 2), was used to estimate k. The resulting $k_P = k - k_B$ was 1.3×10^{-5} s^{-1}, slightly lower than the estimate of 5×10^{-5} determined for the region between the 4-m isobath and the surf zone edge in Grimes et al. (2021). This k_P is an order of magnitude greater than k_B. The optimal Dirichlet boundary conditions for the 1D models were found to be $C_0 = 0.008$ for the 1D model, $C_0 = 0.01$ for the 1DR model, and $C_0 = 0.011$ for the 1DC model (where 0.01 is 1 part dye to 100 parts water).

Figure 2. a) SD Bight model alongshore-varying alongshore velocity, v_C, as a function of time and y, with alongshore beach locations on right side (compare with Fig. 1). b) Time series of $\bar{v}_\mathrm{C}$ (black) with v_1D (blue), c) Time series of $\bar{v}_\mathrm{C}$ with v_1DR (green), d) scatter plot of hourly $\bar{v}_\mathrm{C}$ vs v_1D, best fit line (black dashed line) has slope = 1.02, intercept = −0.0022, and R = 0.89, e) scatter plot of $\bar{v}_\mathrm{C}$ vs v_1DR, best fit line (black dashed) has slope = 1.02, intercept = −0.0015, and R = 0.82. One-to-one line (magenta) for comparison with best fit in d) and e). RMS of $\bar{v}_\mathrm{C}$ is 0.1 m s^{-1}.

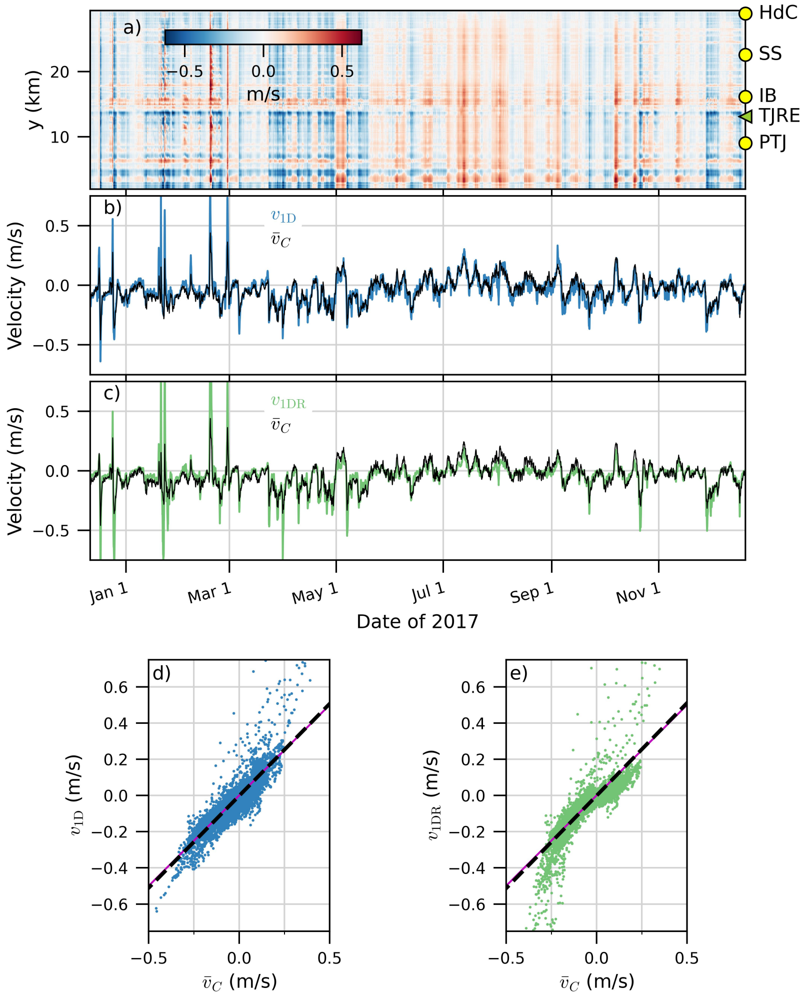

3.3 Reproducing event-scale nearshore dye

An example of a south swell event occurred in the SD Bight model in early July, 2017, when dye was present along the entire alongshore span of the nearshore region (snapshot at July 11, 2017 12:00:00 in Fig. 1c). To demonstrate the evolution of this event in the SD Bight model and the 1D model, the nearshore currents and dye concentrations were examined for the four days leading up to that snapshot (Fig. 4). For this demonstration, we do not depict the 1DR or 1DC models because 1D model results are typical. On July 8, before the swell, $C_\mathrm{C} < 10^{-4}$ north of $y = 2$ km and nearshore cur-

Figure 3. Nearshore dye concentrations averaged over the year 2017 as a function of y for the SD Bight model (solid black line) and the 1D (blue), 1DR (green), and 1DC (orange) models. The 1D, 1DR, and 1DC models used the same k_B and k_P but different C_0. An e-folding decay length scale of 7.9 km was derived using a linear fit to the log of $\langle C_C \rangle$ from $y = 5$ to 29 km (dashed black line), implying a decay rate of $k_P = 1.4 \times 10^{-5} \mathrm{s}^{-1}$. Dashed green line is location of TJRE mouth and beaches are marked as on other figures.

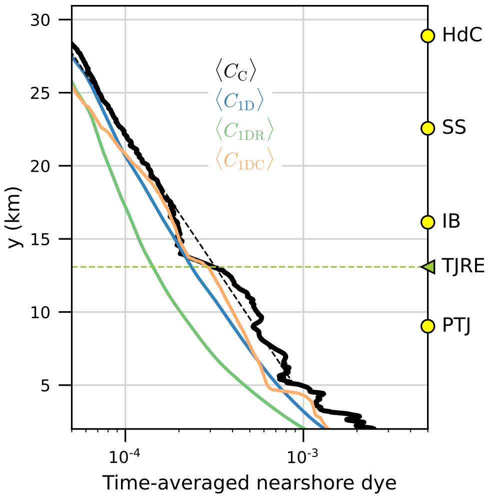

rents were near zero. Over three days, a steady wave-driven current over 10 cm s^{-1} advected the plume 10 km per day until the plume front reached HdC (Fig. 4a, b). Dye concentrations were highest near PB ($C_C \approx 10^{-2}$) and became more dilute downstream ($C_C \approx 10^{-4}$ at HdC) (Fig. 4b). The wave-driven nearshore alongshore current, v_{1D}, was very similar in magnitude and timing to $\bar{v}_C$ (Fig. 4a), consistent with the high skill over the course of the year (Fig. 2b). The 1D model, using v_{1D}, reproduced the plume event. The plume front moved up the coast at the same rate, from $C_{1D} < 10^{-4}$ on July 8, 2017 to $C_{1D} > 10^{-4}$ found at y >20 km on July 11, 2017 (Fig. 4c). The 1D model, composed of solely wave-driven advection and loss, could largely reproduce the July 11, 2017 snapshot from the SD Bight model.

3.4 Comparison of dye performance using different velocity estimates

Here we compare the performance of the 1D model with the 1DR model. The two models use the same numerical scheme but different formulas for the nearshore alongshore velocity (see Section 2.4). The rate of dye loss $k = k_P + k_B$ was the same, but the dye input, C_0, was optimized for separate runs (see Section 2.2).

The dye from the 1D model, C_{1D}, and the 1DR model, C_{1DR}, were compared with C_C for the alongshore region $y > 0$ km over the entire year (Fig. 5). Seasonal patterns

Figure 4. a) Time series of $\bar{v}_{\mathrm{C}}$ (black) and v_{1D} (blue). Evolution as a function of y and t of b) C_{C} and c) C_{1D}. Black dashed line indicates July 11, 2017 12:00:00, time of the snapshot in Fig. 1c. Dashed contour $C_{\mathrm{BAC}} = 5 \times 10^{-4}$ in a) and c).

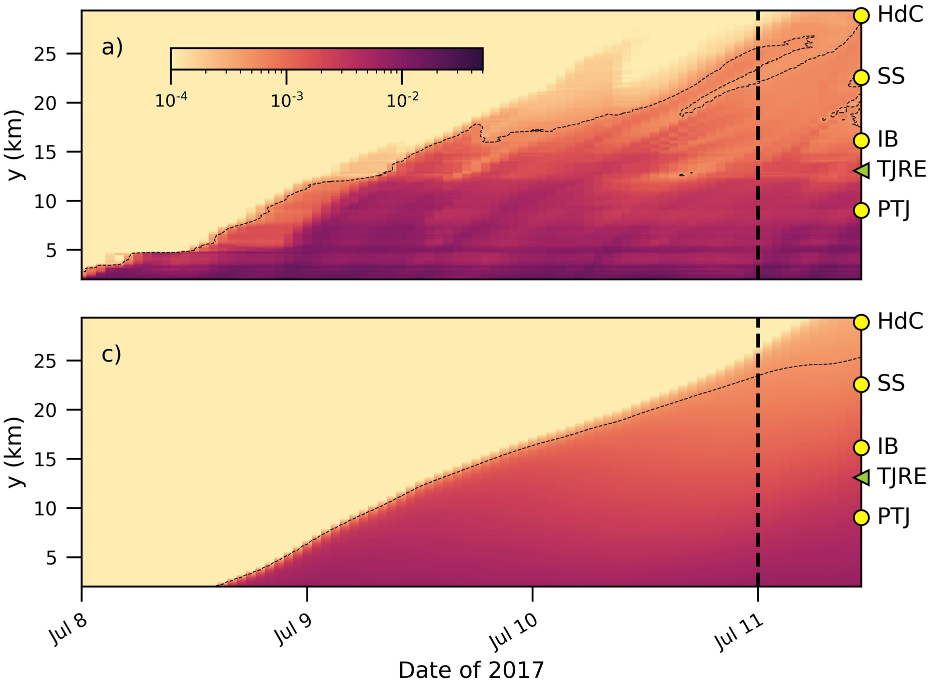

447 in C_{C} were reproduced in both C_{1D} and C_{1DR}. More dye was transported northward during summer months (between June 1 and October 1) than non-summer months in all models. Both C_{C} and C_{1D} reached $y > 20$ km most frequently in summer (Fig. 5a,b). Dye plumes that reached $y > 20$ km during summer exceeded C_{BAC} for many days, often up to a week. The example plume from July 11 (Fig. 4) reached $y > 20$ km in all three models and concentrations remained above C_{BAC} for 3.5 days in the 1DR model, 6 days in the 1D model, and 8 days in the SD Bight model. For comparison, during a plume that reached $y > 20$ km in all three models beginning February 28, concentrations exceeded C_{BAC} for just 2 days in all three models, typical for winter conditions. In the SD Bight model, C_{C} remained longer than C_{1D} at intermediate concentrations between 10^{-8} and C_{BAC} because dye could recirculate back into the nearshore from offshore, which was not possible in the 1D or 1DR models (Fig. 5a). More dye was transported northward during summertime because alongshore nearshore velocity was persistently northward, even though the fastest alongshore velocities occurred in winter (Fig. 2b, c). In winter, northwesterly waves drive predominantly southward nearshore alongshore currents resulting in less dye transport in all models, despite episodic south swells driving nearshore alongshore currents greater than 0.5 m s^{-1}. The 1DR model transported less dye in summertime than the 1D model because v_{1DR} underestimated summertime northward cur-

rents (Fig. 2d). Between June 1 and October 1, the 1D model transported 6.6 times more dye north of $y = 20$ km than the 1DR model.

Figure 5. Dye concentration, $C(t, y)$, for $y > 0$ km and for the entire year from a) the SD Bight model, b) the 1D model, and c) the 1DR model. Dashed contour is C_{BAC}.

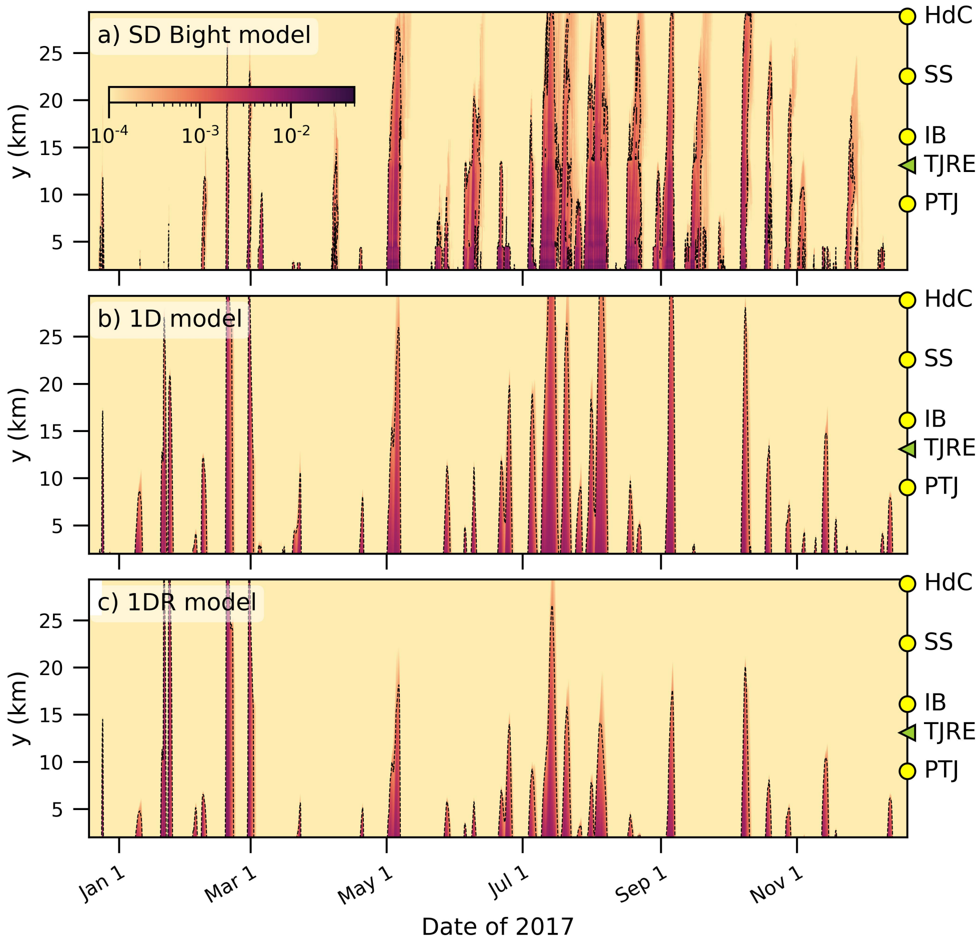

The three performance metrics (R, NRMSE, and WSS) as a function of y statistically quantified the ability of the 1D, 1DR, and 1DC model runs to reproduce the nearshore dye concentrations from the SD Bight model (Fig. 6). The 1DC model run (orange line in Fig. 6) used the exact alongshore velocity from the SD Bight model, demonstrating an upper limit on performance for the 1D and 1DR models, which used wave-driven velocities. The 1DC model performance did not drop at the TJRE, but remained approximately constant with alongshore distance until $y = 27$ km. North of $y = 27$ km, 1DC model skill decreased because the shoreline curvature increases (Fig. 6). The 1D model performed much better than the 1DR model (compare blue line with green in Fig. 6). The 1D model had an approximately constant WSS = 0.75 south of the TJRE (Fig. 6c).

Both the 1D and 1DR models decrease in skill at the TJRE, with a drop in R and WSS of about 0.15 (Fig. 6a, c). The 1DR model performed the worst, decaying rapidly with y. All further analyses will consider only the 1D model.

Figure 6. Model performance metrics comparing $C_{1\mathrm{D}}$ (blue), $C_{1\mathrm{DR}}$ (green) and $C_{1\mathrm{DC}}$ (orange) with C_{C} as a function of y. a) R, b) NRMSE, c) WSS. Green dashed line is location of TJRE. Markers on the right indicate alongshore locations of beaches seen in Fig. 1.

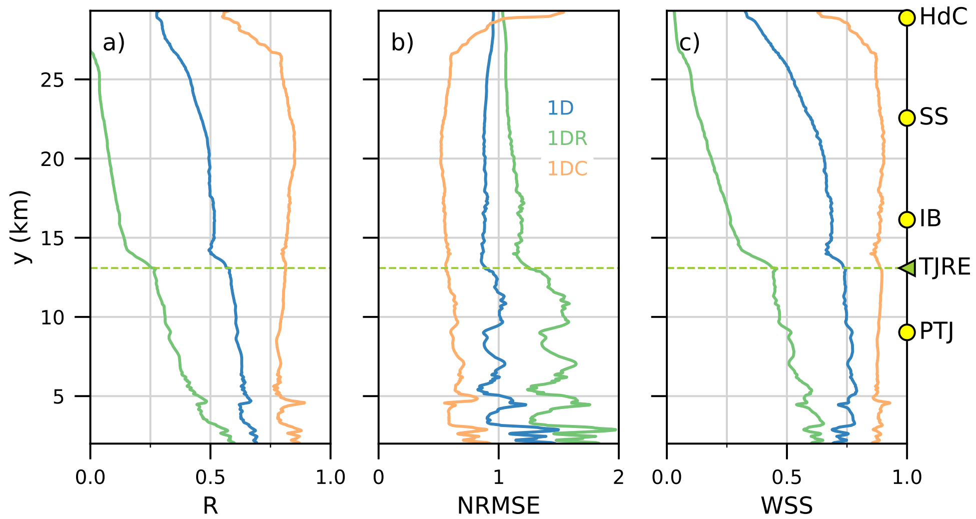

The 1D model and SD Bight model had similar counts of time steps when dye exceeded C_{BAC}, but the SD Bight model had more time steps when dye concentrations were between 10^{-8} and C_{BAC} (Fig. 7). Dye in the 1D model was more often near zero than between 10^{-8} and C_{BAC} (Fig. 7). Intermediate dye concentrations between 10^{-8} and C_{BAC} in the SD Bight model may be partly due to dye recirculation from the inner shelf, a process not included in the 1D model. Some of the error in 1D model performance is then accounted for by these missing intermediate dye concentrations. However, intermediate concentrations are below the beach advisory condition threshold by definition, so the absence of intermediate dye concentrations in the 1D model is not a significant concern for potential public health applications.

3.5 Model binary performance using a cutoff value

Dye plume events were counted using the C_{BAC} threshold in a time series of $C_{1\mathrm{D}}$ and C_{C} at IB (Fig. 8). This first analysis focuses only on the summer months, June 1 to October 1, when beach tourism is elevated and SABWTP plume occurrences are most

Figure 7. Horizontally stacked, normalized histogram of occurrences of dye values in a) the 1D model and b) the SD Bight model. Color represents dye concentration bins (colormap similar to dye colormap in previous figures but with added distinction between values greater than or less than 10^{-8}). Contours delineate three bins (less than 10^{-8}, 10^{-8} to $C_{\mathrm{BAC}} = 5 \times 10^{-4}$, and greater than $C_{\mathrm{BAC}} = 5 \times 10^{-4}$).

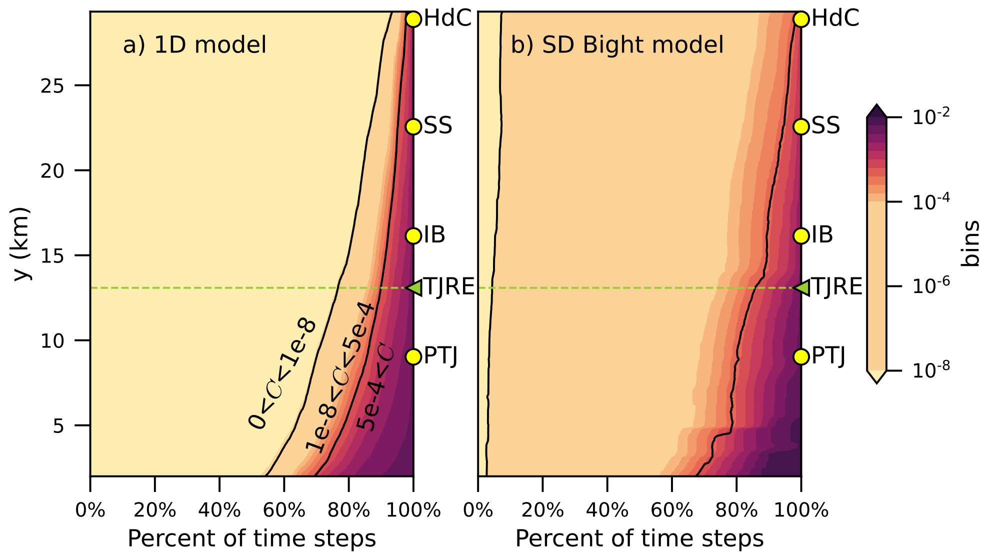

frequent (Feddersen et al., 2021). Four conditions are defined using a binary logic criteria of dye greater than C_{BAC}, taking C_{C} as the true result,

1. True Positive: both $C_{\mathrm{1D}} > C_{\mathrm{BAC}}$ and $C_{\mathrm{C}} > C_{\mathrm{BAC}}$
2. False Positive: $C_{\mathrm{1D}} > C_{\mathrm{BAC}}$ but $C_{\mathrm{C}} < C_{\mathrm{BAC}}$
3. False Negative: $C_{\mathrm{1D}} < C_{\mathrm{BAC}}$ but $C_{\mathrm{C}} > C_{\mathrm{BAC}}$
4. True Negative: both $C_{\mathrm{1D}} < C_{\mathrm{BAC}}$ and $C_{\mathrm{C}} < C_{\mathrm{BAC}}$

If a plume is True Positive at any time during its stay, it was counted as a True Positive plume even if it had adjacent periods of False Positive or False Negative. Using this binary analysis, eight distinct summertime plumes are counted at IB (Fig. 8). There were four True Positive plumes (beginning July 11, July 16, July 31, and August 2), two False Positive plumes (beginning June 23 and July 4), and two False Negative plumes (beginning June 8 and August 18) (Fig. 8). The True Positive plumes were sometimes preceded by a brief False Negative period and followed by a brief False Positive period, because the plumes in the SD Bight model arrived earlier and retreated earlier.

Figure 8. Dye concentrations at Imperial Beach (yellow circle labelled IB in Fig. 1) over three summer months from the SD Bight model (black solid line) and 1D model (blue solid line). The dashed red line indicates $C_{\mathrm{BAC}} = 5 \times 10^{-4}$. Colored bars at top of figure depict True Positive, (purple), False Positive (orange), False Negative (blue), or True Negative (white). Four conditions defined in text.

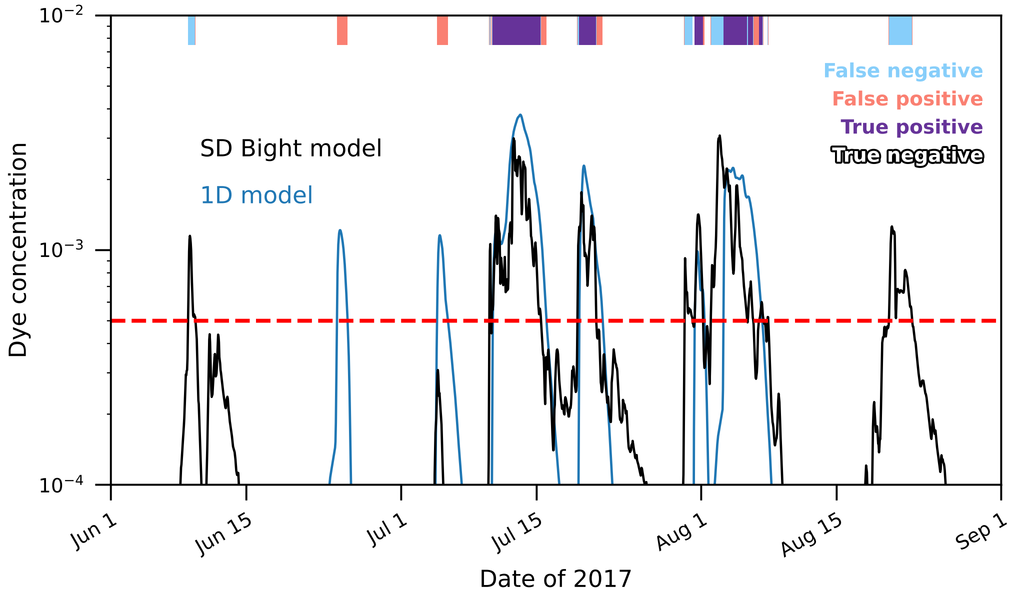

Next, the binary analysis was extended to all shoreline locations and all time steps (Fig. 9). Agreement was defined as the combined number of hourly time steps that had True Positive or True Negative conditions, and disagreement was either False Positive or False Negative conditions. The 1D model and SD Bight model were in agreement for 89% of all time steps at all alongshore locations (Fig. 9c). The most common condition was True Negative, accounting for 75% of all hourly time steps at all locations. True Positives were 14%, False Positives were 7%, and False Negatives were 4%. Disagreement was seasonal. During summer, False Negatives were more likely, rising to account for 14% of time steps between June 1 and October 1. During all other months, however, False Negatives and False Positives were equally likely, occurring in between 4 to 5% of non-summer time steps. The percent of time steps in agreement increased with y (Fig. 9c), in contrast to the pattern in model skill (Fig. 6). This increase is due to an increase in True Negatives with y (Fig. 9b). True Negatives accounted for 95% of time steps north of $y > 20$ km because dye concentrations exceeding C_{BAC} rarely reached $y > 20$ km in either model.

Figure 9. a) Time series comparing the binary conditions $C_C > C_{BAC}$ and $C_{1D} > C_{BAC}$ as a function of y for model year 2017, b) horizontal stacked bar plot of percentage of occurrences of the four conditions as a function of y, c) percent of all time steps that are True Positive or True Negative as a function of y. Four conditions defined in text.

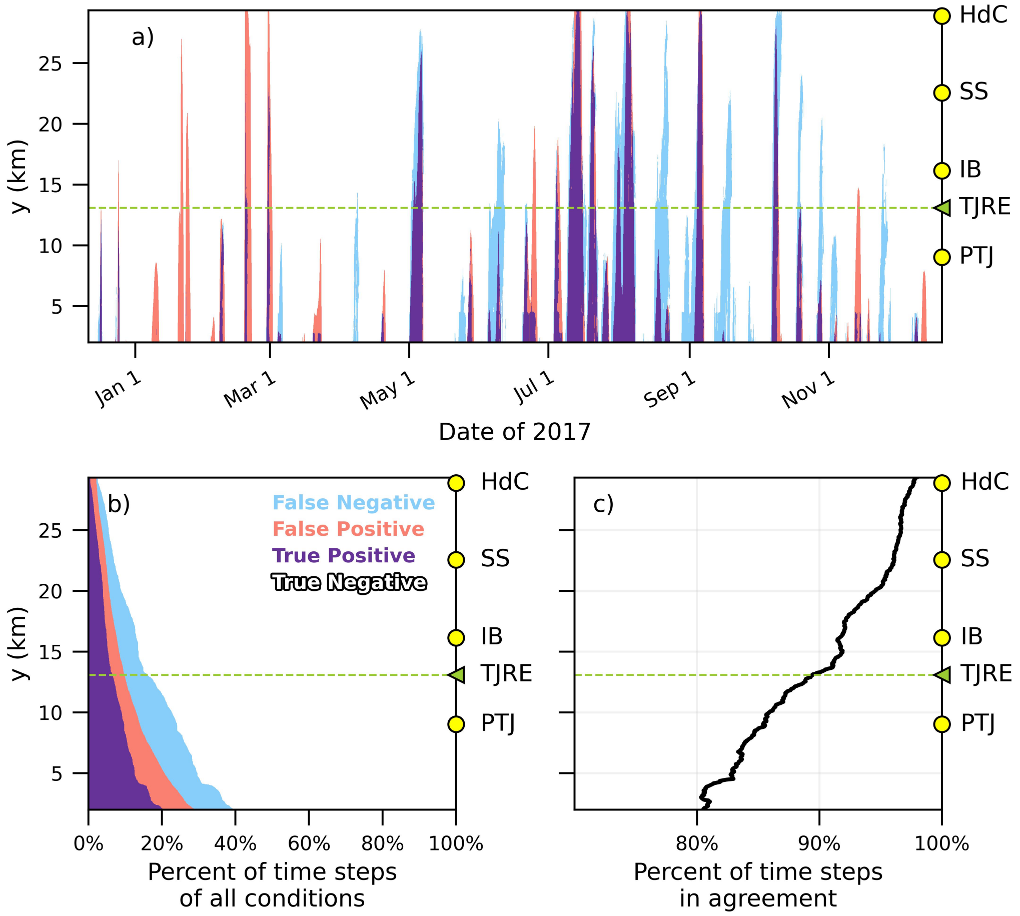

3.6 Daily beach advisories: comparing 1D model forecast with simulated weekly sampling

The previous analysis considered hourly agreement in the binary analysis, but in practice, agreement on a daily time scale would be most relevant for beach managers because beach advisories are issued daily. Currently, daily beach advisories in San Diego are informed in part by weekly sampling for FIB performed at major beaches (San Diego County, n. d.). Samples are sent to labs for analysis and if FIB are found, beach advisories can be issued the next day (Francy, 2009). A weekly sampling schedule is currently the minimum frequency recommended for water quality monitoring at heavily used urban beaches by the U.S. Environmental Protection Agency (U.S. Environmental Protection Agency, 2014). However, a study on FIB sampling frequency at beaches in Los Angeles, CA, found that a weekly testing schedule missed up to 75% of FIB exceedances, which frequently lasted only one day (Leecaster & Weisberg, 2001). Further, a probabilistic model estimated that up to 40% of beach advisories at Huntington Beach, CA, are incorrectly posted (J. Kim & Grant, 2004). Although here dye was modeled with the 10-day decay rate of norovirus, weekly sampling is still likely to misrepresent dye presence because dye concentrations were determined primarily by alongshore advection, which acted on shorter time scales. We compared the accuracy of daily beach advisories informed by hourly 1D model predictions with a simulation of a weekly sampling schedule using the SD Bight model. For this experiment, the ideal daily beach advisory was issued at an alongshore location if $C_{\mathrm{C}} > C_{\mathrm{BAC}}$ for at least one hour during that day. A 1D model-informed daily beach advisory was issued at an alongshore location if $C_{\mathrm{1D}} > C_{\mathrm{BAC}}$ for at least one hour during that day. To simulate weekly sampling, C_{C} was checked at one time step once per week. If that sample exceeded C_{BAC}, a daily beach advisory was issued the following day (to match the time lag required to process samples) and remained in place for the next seven days until the next sample was processed. Accuracy was determined by checking if the 1D model-informed and simulated weekly sampling-informed daily beach advisories matched the ideal beach advisory. The magnitude and shape of the curve for 1D model-informed daily beach advisory accuracy (Fig. 10) were consistent with the hourly agreement between binary metrics $C_{\mathrm{C}} > C_{\mathrm{BAC}}$ and $C_{\mathrm{1D}} > C_{\mathrm{BAC}}$ (Fig. 9b). The range of accuracy of simulated weekly sampling-informed daily beach advisories found here (Fig. 10) was consistent with the range of 0–40% inaccuracy in daily beach advisories estimated for Huntington Beach, CA (J. Kim & Grant, 2004). The 1D model-informed daily beach advisories were more accurate than simulated weekly sampling at all locations, averaging 87% accuracy over all time steps and 10% improvement over simulated weekly sampling (Fig. 10). Similar to the hourly count, accuracy for both 1D model-informed and simulated weekly sampling-informed daily beach advisories increased with y as distance from the point source, and thus true positives decreased.

4 Discussion

There is a growing understanding of the need to supplement *in situ* sampling with predictive modeling nowcasts (Francy, 2009). Although predictive modeling of waterborne pathogens has been a concern for decades, the majority of operational predictive water quality models are regressive rather than mechanistic (Elko et al., 2022). Regressive models predict FIB concentrations using statistically correlated factors, such as rainfall (de Brauwere et al., 2014). The San Diego-Tijuana region nearshore is frequently contaminated with untreated sewage from SABWTP transported by wave-driven currents (ARCADIS, 2019), producing a swimmer illness hazard than must be modeled mecha-

Figure 10. Percent agreement with ideal daily beach advisories (days when $C_{\mathrm{C}} > C_{\mathrm{BAC}}$ for any hourly time step) of simulated weekly sampling-informed daily beach advisories (pink) and 1D model-informed daily beach advisories (blue).

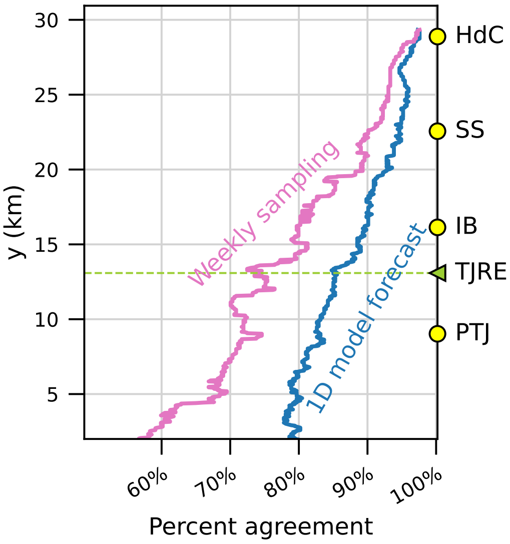

nistically. Here, we demonstrated that a simple tracer advection model using only wave-driven alongshore currents does a good job of reproducing nearshore transport of a tracer from a 3D hydrodynamic model of the San Diego-Tijuana coastline. A simple 1D nearshore transport model could improve existing shoreline exposure modeling that uses only HFR-derived shelf currents (S. Y. Kim et al., 2009; Rogowski et al., 2015) and could be tuned and operational as a forecast much more quickly than a 3D hydrodynamic model (Wu et al., 2020). Nearshore momentum has been observed to be dominated by wave-forcing (Lentz et al., 1999; Feddersen, 1998), and a wave-only model has the advantage of the availability of wave forecasts at existing wave buoys. Previous 1D tracer advection models of the nearshore environment have been used to estimate the transport of wastewater (Boehm, 2003) and dye (Grimes et al., 2021), but these have been evaluated over limited conditions. With the spatial and temporal resolution of the SD Bight model hindcast for 2017, we could produce a detailed evaluation of the 1D model performance for both velocity and dye across a variety of seasonal forcing conditions and realistic shoreline features. A binary analysis of presence or absence of tracer concentrations in the 1D model above a cut off relevant for human health, $C_{\mathrm{BAC}} = 5 \times 10^{-4}$, was in agreement with the SD Bight model for 89% of all hourly time steps over all y. Here we summarize and expand upon our results and discuss applicability to other locations.

4.1 Comparison of velocity formulas

Nearshore alongshore velocity was modeled with two different bottom stress formulas using wave properties at an offshore wave buoy location. The first, v_{1D}, used the small angle, weak current approximation (Wright & Thompson, 1983) and the second, v_{1DR}, used a further simplified linear Rayleigh friction (Lentz et al., 1999; Feddersen et al., 2000). The scaling difference between the formulas is that $v_{\mathrm{1D}} \propto H_{s,5\mathrm{m}}^{-1} S_{xy}$ (11) and $v_{\mathrm{1DR}} \propto S_{xy}$ (12). Once tuned for their respective drag coefficients, both modeled velocities had good agreement (R > 0.8) with the alongshore-mean nearshore alongshore velocity, $\bar{v}_{\mathrm{C}}$, extracted from the SD Bight model. The velocity estimated using Rayleigh friction, v_{1DR}, had an R value 0.07 lower than v_{1D}. Rayleigh friction models do not capture extremes well, underestimating slow currents and overestimating fast currents (Feddersen et al., 2000), as found here where the 1DR model velocity, v_{1DR}, underestimated slow summertime alongshore nearshore velocities (Fig. 2c). Due to this underestimate, the 1DR model could not reproduce summer dye plumes when transport was most frequently northward (Fig. 5c). Re-tuning v_{1DR} to fit only summertime nearshore alongshore velocities would likely improve overall performance of the 1DR model dye transport, but we wanted to demonstrate the results of tuning to available data without *a priori* assumptions about the relative importance of seasonal conditions for model performance. Lentz et al. (1999) found good agreement between Rayleigh friction-estimated wave-driven velocities and observations, but they did not attempt to model tracer transport. Even though the decrease in velocity correlation was small, the decrease in dye transport skill was substantial (compare blue line with green line in Fig. 6). Errors in Lagrangian quantities are magnified from errors in velocity because instantaneous velocity is integrated in space and time. Grimes et al. (2021) had success with a Rayleigh friction model, however they only modeled dye transport over a 30 hour time period during which H_s was approximately constant. Other bottom stress formulas that include strong current limits were tested (Wright & Thompson, 1983; Feddersen et al., 2000), but did not capture the extreme winter events better than v_{1D}. Further model improvement to reduce the overestimation of nearshore alongshore velocities during large southerly swells may not improve model transport much overall because northward currents are typically weak.

Only wave-driven velocities were included here to optimize performance with simplicity. However, model performance would likely be further increased by including wind stress in the velocity formulas. Wind stress has been observed to be the second leading-order term in the nearshore alongshore momentum balance, after wave forcing (Feddersen, 1998; Lentz et al., 1999). The improvement in model performance by including wind here is likely to be small since winds in this region were light, with subtidal wind speeds less than 2 ms^{-1} in 2017 (not shown). However, wind stress may be more important for nearshore transport in other regions. For example, in Melbourne Beach, FL, where hurricanes are common, the correlation of wind stress with waves explained net sediment transport better than waves alone (Burnette & Dally, 2018).

4.2 Skill in reproducing tracer distributions

For the problem of nearshore alongshore transport of SABWTP wastewater in the San Diego-Tijuana region, a 1D grid has been demonstrated to be an effective alternative to a realistic 3D hydrodynamic model. Grimes et al. (2021) found that differentiating and including re-circulation between the surf zone and the inner-shelf (i.e., a 2 box model in the cross-shore direction) increased the performance of a 1D wave-advection model in reproducing the transport of a single dye plume through the surf zone over 30 hours. In contrast, here exchange with the inner shelf was parameterized as monotonic loss, but the time scale considered was expanded to include dozens of plume events over the course of a year. Even with this simplified parameterization of exchange (i.e., loss only, no re-circulation) with the shelf, the 1D dye advection-loss model could reproduce SD Bight model nearshore dye concentrations with considerable skill (Fig. 6). The 1DC model demonstrated that, with perfect knowledge of nearshore currents, a uniform 1D grid and simple dye loss parameterization could reproduce nearshore tracer concentrations from the SD Bight model with a WSS = 0.9, and with no reduction of WSS around the TJRE (Fig. 6c). The 1DC model performance decreased in all metrics for $y > 27$ km (Fig. 6) where shoreline curvature increases (Fig. 1) and nearshore alongshore velocity slows (Fig. 2). Tracer advection in this region may be underestimated by not including angular acceleration along the curving shoreline. Alternatively, slower nearshore alongshore advection of tracer may be compensated for in the SD Bight model by inner shelf tracer steered back into the nearshore along the more tightly-curved 10- and 20-m isobaths (Fig. 1), a process missing from the 1DC model. Using a wave-driven, alongshore-uniform, nearshore alongshore velocity, the 1D model WSS was only 10% less than the 1DC model on average (Fig. 6). The 1D and 1DR model performances were lower downstream of the TJRE (Fig. 6). This decreased performance may be attributed to low dye concentrations which are less likely to be a public health concern than high dye concentrations. This explanation is supported by analysis of 1D and SD Bight model dye using the binary condition of dye exceeding C_{BAC}. In the binary analysis, agreement between the 1D model and the SD Bight model increased with y (Fig. 9). These low dye concentrations missing from the 1D model may arise from tidal trapping diffusion or recirculation of dye into the nearshore from the inner shelf. Recirculation is likely a less significant contributor of low dye concentrations than tidal trapping, since recirculation was not included in the 1DC model which did not decrease in performance downstream of the TJRE mouth. Future work is needed to explicitly explore the dynamical role of inlets and shoals on nearshore alongshore tracer transport.

The 1D model equation used here (5) did not include alongshore diffusivity, unlike similar 1D models of nearshore alongshore advection (e.g., Grant et al., 2005; Grimes et al., 2021). This is because numerical alongshore diffusivity arising from the upwind advection scheme provided adequate alongshore diffusivity expected for this environment. The numerical alongshore diffusivity, K^*_{yy}, was estimated using a scale analysis,

$$K^*_{yy} \approx \frac{V \Delta y}{2} \tag{14}$$

where Δy was the grid cell length. For this 1D model, the numerical $K^*_{yy} = 1.5$ m^{2}s^{-1}. Estimation of expected alongshore diffusivity follows Spydell et al. (2009), who calculated nearshore alongshore diffusivity using drifters at Huntington Beach, CA and Torrey Pines, CA over a nearshore domain which extended beyond the surf zone to an offshore distance of 160 m. Spydell et al. (2009) used two scaling estimates of K_{yy}. The first calculation used mixing length arguments (Tennekes & Lumley, 1972),

$$K_{yy} \approx \gamma V L, \tag{15}$$

where $V = 0.1$ m s^{-1} was used as a typical velocity scale (RMS of $\bar{v}_{\mathrm{C}}$, see Fig. 2) and γ is a fitting parameter, found in Spydell et al. (2009) to be $\gamma = 0.52 \pm 0.08$. The second calculation used shear dispersion in a pipe (Taylor, 1953; Spydell et al., 2007),

$$K_{yy} \approx V^2 T_0, \tag{16}$$

where T_0 is the timescale of mixing, found in Spydell et al. (2009) to be $T_0 = 154 \pm 13$ s. Using V and L in this study results in K_{yy} estimates of 10 and 1.5 m^{2}s^{-1} for the mixing length and pipe shear dispersion arguments, respectively. This range is consistent with the range of $K_{yy} = 1 - 10$ m^{2}s^{-1} estimated in Grimes et al. (2021). Grant et al. (2005) found significantly higher estimates of $K_{yy} = 40{-}80$ m^{2}s^{-1} in their field observations at Huntington Beach, CA (same study location as Spydell et al., 2009), but Grant et al. (2005) considered only the well-mixed region of the surf zone extending to 50 m offshore. The numerical diffusivity K^*_{yy} falls within the range of expected alongshore diffusivity found here, $K_{yy} = 1.5 - 10$ m^{2}s^{-1}. Inclusion of additional prescribed alongshore diffusivity was tested using K_{yy} ranging from 1 to 10 m^{2}s^{-1}, but model performance metrics varied by at most 3% of their original values. This justified neglecting additional alongshore diffusivity beyond numerical alongshore diffusivity.

4.3 Impact of non-uniform bathymetry on alongshore transport

Model skill was hypothesized to decrease downstream of the TJRE because complex dynamics near the TJRE mouth could not be represented in a simple 1D advection model. The 1DC model did not decrease in skill at the TJRE (Fig. 6), likely because the velocities extracted from the SD Bight model already incorporate modulations caused by the estuary presence (both bathymetric steering and tidal currents). The 1D and 1DR models did have small performance drops of 0.15 in R and WSS at the TJRE (kinks in blue and green solid lines at green dashed line Fig. 6). Together, these results suggest the TJRE produces an anomaly in the wave-driven alongshore velocity. The TJRE is a site of persistent divergence in the alongshore-varying nearshore alongshore velocity time series, most pronounced in non-summer months (Fig. 2a). The divergence arises between the TJRE and IB, where there is the shoal (visible north of the TJRE mouth in 10-m isobath contour in Fig. 1). The shoal affects wave-driven currents but may also steer alongshore flow. Divergence may also arise when there is flow out of the TJRE mouth, either from the episodically-flowing Tijuana River or ebb tides. Importantly, there was no decrease at the TJRE in agreement in the binary analysis comparing time steps with dye concentrations exceeding C_{BAC} in the 1D model with the SD Bight model (Fig. 9b). This suggests that discrepancies in small dye concentrations (less than C_{BAC}) account for the decrease in R and WSS in the 1D model downstream of the TJRE (Fig. 6a, c).

4.4 Application for water quality prediction in San Diego-Tijuana region

The 1D model was able to reproduce the concentration of a tracer from a point source throughout a 30 km nearshore region from the SD Bight model, a much more complex COAWST model which includes the alongshore-variable bathymetry and shelf circulation. These model-model comparisons demonstrate the viability of a 1D wave-advection model in predicting individual wastewater plumes over a range of seasonal wave conditions, not only the recreation of specific events. The methods used here to tune nearshore alongshore advection and dye concentrations to SD Bight model values could be applied to historical wave, current, and FIB observations in the San Diego-Tijuana region to build an operational water quality forecast with minimal adjustments. Velocity could be tuned using wave data from the CDIP Imperial Nearshore buoy and observed nearshore currents. To calibrate tracer transport, we could use available historic water sampling data. Only data from the dry season would be used for calibration to isolate the wastewater plume from SABWTP from other pathogen sources, such as the TJRE or storm water runoff (as in Zimmer-Faust et al., 2021). Dye decay parameters could be adapted to match the pathogens tested for in water sampling. Here we used norovirus, but historic water sampling has tested for FIB, *E. Coli*, and *Enterococcus* (San Diego County, n. d.), all of which decay more rapidly than norovirus. The average measured e-folding time scale of *E. Coli* is 2–3 days (Boehm et al., 2018). The decay rate of *Enterococcus* is modulated by UV exposure, with populations decreasing by 90% in 81 minutes when exposed to midday sunlight (Davies-Colley et al., 1994), but in darker, colder environments the decay timescale can lengthen to a few days (Byappanahalli et al., 2012). To reproduce the rate of dye loss for *Enterococcus*, the decay rate would require programmed sunlight dependence.

The 1D model could be used in concert with the existing plume tracker model to improve performance (S. Y. Kim et al., 2009; Rogowski et al., 2015). The offline particle tracking algorithm which currently uses observed shelf currents to model transport of FIB could implement a nested 1D wave-driven nearshore transport model when particles are found within 200 m of the shoreline.

4.5 Applications to other regions and tracers

The 1D wave-advection model tested here was motivated by the problem of wastewater transport in the San Diego-Tijuana nearshore region, but the dynamics of this nearshore region are not unique. This method could be adapted to model the nearshore transport of other tracers on other mostly straight, wave-dominated coastlines using wave buoys. For example, the modeling method could be applied to predict the wave-driven nearshore transport of microplastics (Kerpen et al., 2020). Although here we used a persistent flux of polluted waters, a time-dependent source term could represent transient sources of pollution to wave-dominated coastlines. For example, FIB levels are elevated in rivers in the days following hurricanes in North Carolina (Humphrey et al., 2019; Neville et al., 2021). Those polluted rivers form buoyant plumes at the coast which are partially trapped in the nearshore (Rodriguez et al., 2018; Kastner et al., 2019), and the 1D model could be used to model the wave-driven fate of those plumes along the shoreline. Because the 1D model presented here is simple, it could be coupled to models that currently only use shelf circulation. Offline particle tracking algorithms used to model transport of harmful algal blooms (Giddings et al., 2014) or larvae (Brasseale et al., 2019) using shelf currents could implement a nested nearshore 1D wave-driven transport model as described above for the plume tracker model (S. Y. Kim et al., 2009; Rogowski et al., 2015). With the inclusion of wind stress, this approach could be used to model sediment transport during storms on sandy coastlines, such as hurricanes on the Atlantic coast of Florida (Burnette & Dally, 2018), Nortes on the Yucatan peninsula in Mexico (Medellin et al., 2021; Torres-Freyermuth et al., 2021), and monsoons on the Nha Trang beach in Vietnam (Tran et al., 2021). Similar to discussed above, some tracers would require additional decay/loss terms such as due to sunlight dependence (e.g., *Enterococcus*) or sinking (e.g., sediment).

5 Conclusions

A 1D transport-decay model has been shown to reproduce the mean alongshore currents and nearshore concentrations of a tracer from a 3D hydrodynamic model of the San Diego-Tijuana coastal ocean. This demonstrates the viability of simple 1D models for nearshore water quality prediction and transport of other tracers such as larvae, sediment, or microplastics. Two wave-derived velocity formulas were tested using wave properties from an offshore location. Given the range of wave properties in this region over the twelve-month model period, nearshore tracer evolution could be estimated well using the small angle, weak current approximation, but not with the linear friction approximation. Running the same 1D model using a linear friction model for velocity produced dye distributions with considerably less model skill than the small angle, weak current model. The effect of a small inlet and shoal at the TJRE on alongshore transport was examined. However, model performance was unaffected by the TJRE for values of dye that were above a beach advisory threshold, $C_{\mathrm{BAC}} = 5 \times 10^{-4}$. Only when small (inconsequential from a human health perspective) dye concentrations were considered did model performance decrease by 10% north of the TJRE. Because this 1D wave-advection model can be run with a wave buoy or a wave forecast model, it could be used for real-time or forecasts of tracer transport in other coastal regions. The simplicity, speed, and accuracy of this 1D nearshore model are evidence that a similar modeling technique could be implemented in place of or in concert with a full hydrodynamic model for public health websites and ensemble studies where full hydrodynamic models may be impractical. Moreover, it can be combined with other existing tracer transport models that focus on shelf-circulation to better represent the fate of tracers along the shoreline.

Acknowledgments

Model development was supported by grants from the National Science Foundation (OCE-1459389) as part of the Cross-Surfzone/Inner-shelf Dye Exchange (CSIDE) experiment and the Environmental Protection Agency through the North American Development Bank, however, it does not necessarily reflect the policies, actions or positions of the U.S. EPA, NADB, or NSF. This project is supported by the US Coastal Research Program (USCRP) as administered by the US Army Corps of Engineers (USACE), Department of Defense and in part by NSF OCE-1924005. The content of the information provided in this presentation does not necessarily reflect the position or the policy of the government, and no official endorsement should be inferred. The authors' acknowledge the USACE and USCRP's support of their effort to strengthen coastal academic programs and address coastal community needs in the United States. NOAA provided the hydrodynamic model atmospheric forcing fields and the bathymetry. SIO Coastal Data Information Program provided wave forcing. Ganesh Gopalakrishnan and Bruce Cornuelle provided CASE model solutions for outer grid boundary conditions which are available online (http://ecco.ucsd.edu/case.html). We also appreciate extra support from the Tijuana River National Estuarine Research Reserve, Southern California Coastal Ocean Observing System, and the City of Imperial Beach. Model development and production involved significant contributions from Dr. Jacqueline McSweeney and Dr. Nirnimesh Kumar. We also thank the SIO Center for Coastal Studies and the Navy Marine Ecological Consortium technicians, contractors, and field crew as well as all of the volunteers who helped collect observations that were used for the 3D hydrodynamic model validation. Finally, useful conversations regarding data processing and analysis was provided by several individuals, especially Katharine Ricke, Pascal Polonik, Derek Grimes, Duncan Wheeler, Samuel Kastner, Emily Lemagie, Katherine Hewett, and Alexandra Simpson. Code used to process COAWST ouptut, run 1D models, and analyze data presented in plots is available at DOI:10.5281/zenodo.6544844. 1D model output and SD Bight model extracted and processed nearshore data is in the process of being made publicly available on the UCSD Digital collections library, and will have a citable DOI before publication of this manuscript.

References

Aguilera, R., Gershunov, A., & Benmarhnia, T. (2019). Atmospheric rivers impact california's coastal water quality via extreme precipitation. *Science of the Total Environment*, *671*, 488–494. doi: https://doi.org/10.1016/j.scitotenv.2019.03.318

ARCADIS. (2019). *Tijuana river diversion study* (Tech. Rep.). San Antonio TX: North American Development Bank. (`https://www.nadb.org/uploads/files/tijuana_river_diversion_study_final_report_full_sm.pdf`)

Banas, N., MacCready, P., & Hickey, B. (2009). The columbia river plume as cross-shelf exporter and along-coast barrier. *Continental Shelf Research*, *29*(1), 292–301. doi: https://doi.org/10.1016/j.csr.2008.03.011

Boehm, A. (2003). Model of microbial transport and inactivation in the surf zone and application to field measurements of total coliform in northern orange county, california. *Environmental Science & Technology*, *37*(24), 5511-5517. doi: 10.1021/es034321x

Boehm, A., Ashbolt, N., Colford, J., Dunbar, L., Fleming, L., Gold, M., ... Weisberg, S. (2009). A sea change ahead for recreational water quality criteria. *Journal of Water and Health*, *7*, 9–20. doi: https://doi.org/10.2166/wh.2009.122

Boehm, A., Graham, K. E., & Jennings, W. C. (2018). Can we swim yet? systematic review, meta-analysis, and risk assessment of aging sewage in surface waters. *Environmental Science & Technology*, *52*(17), 9634-9645. doi: 10.1021/acs.est.8b01948

Boehm, A., Keymer, D. P., & Shellenbarger, G. G. (2005). An analytical model of enterococci inactivation, grazing, and transport in the surf zone of a marine beach. *Water Research*, *39*(15), 3565-3578. Retrieved from `https://www.sciencedirect.com/science/article/pii/S0043135405003611` doi: https://doi.org/10.1016/j.watres.2005.06.026

Boehm, A., & Soller, J. (2020). Refined ambient water quality thresholds for human-associated fecal indicator hf183 for recreational waters with and without co-occurring gull fecal contamination. *Microbial Risk Analysis*, *16*, 100139. doi: https://doi.org/10.1016/j.mran.2020.100139

Booij, N., Ris, R. C., & Holthuijsen, L. H. (1999). A third-generation wave model for coastal regions: 1. model description and validation. *Journal of Geophysical Research: Oceans*, *104*(C4), 7649-7666. doi: 10.1029/98JC02622

Brasseale, E., Grason, E., McDonald, P., Adams, J., & MacCready, P. (2019). Larval transport modeling support for identifying population sources of european green crab in the salish sea. *Estuaries and Coasts*, *42*, 1586–1599. doi: 10.1007/s12237-019-00586-2

Burnette, C., & Dally, W. (2018). The longshore transport enigma and analysis of a 10-year record of wind-driven nearshore currents. *Journal of Coastal Research*, *34*, 26–41. doi: 10.2112/JCOASTRES-D-17-00010.1

Byappanahalli, M., Nevers, M., Korajkic, A., Staley, Z., & Harwood, V. (2012). Enterococci in the environment. *Microbiology and Molecular Biology Reviews*, *76*, 685–706. doi: 10.1128/MMBR.00023-12

Cho, K., Cha, S., Kang, J., Lee, S., Park, Y., Kim, J., & Kim, J. (2010). Meteorological effects on the levels of fecal indicator bacteria in an urban stream: A modeling approach. *Water Research*, *44*, 2189–2202. doi: https://doi.org/10.1016/j.watres.2009.12.051

Davies-Colley, R., Bell, R., & Donnison, A. (1994). Sunlight inactivation of enterococci and fecal coliforms in sewage effluent diluted in seawater. *Applied and Environmental Microbiology*, *60*, 2049–2058. doi: 10.1128/aem.60.6.2049-2058.1994

de Brauwere, A., Ouattara, N., & Servais, P. (2014). Modeling fecal indicator bacteria in natural surface waters: A review. *Critical Reviews in Environmental Science and Technology*, *44*, 2380–2453. doi: 10.1080/10643389.2013.829978

Elko, N., Foster, D., Kleinheinz, G., Rubenheimer, B., Brander, S., Kinzelman, J., ... Simm, J. (2022). Coastal forum: Human and ecosystem health in coastal systems. *Shore and Beach*, *90*, 64–91. doi: http://doi.org/10.34237/1009018

Feddersen, F. (1998). Weakly nonlinear shear waves. *J. Fluid Mech.*, *372*, 71-91.

Feddersen, F., Boehm, A., Giddings, S., Wu, X., & Liden, D. (2021). Modeling untreated wastewater evolution and swimmer illness for four wastewater infrastructure scenarios in the san diego-tijuana (us/mx) border region. *GeoHealth*, *5*, e2021GH000490. doi: https://doi.org/10.1029/2021GH000490

Feddersen, F., Guza, R. T., Elgar, S., & Herbers, T. H. C. (2000). Velocity moments in alongshore bottom stress parameterizations. *J. Geophys. Res.*, *105*, 8673-8686. doi: 10.1029/2000JC900022

Feddersen, F., Olabarrieta, M., Guza, R. T., Winters, D., Raubenheimer, B., & Elgar, S. (2016). Observations and modeling of a tidal inlet dye tracer plume. *Journal of Geophysical Research: Oceans*. doi: 10.1002/2016JC011922

Francy, D. (2009). Use of predictive models and rapid methods to nowcast bacteria levels at coastal beaches. *Aquatic Ecosystem Health and Management*, *12*, 177–182. doi: https://doi.org/10.1080/14634980902905767

Giddings, S., MacCready, P., Hickey, B., Banas, N., Davis, K., Siedlecki, S., ... Connolly, T. (2014). Hindcasts of potential harmful algal bloom transport pathways on the pacific northwest coast. *Journal of Geophysical Research-Oceans*, *119*(4),

2439-2461. doi: https://doi.org/10.1002/2013JC009622
Grant, S. B., Kim, J. H., Jones, B. H., Jenkins, S. A., Wasyl, J., & Cudaback, C. (2005). Surf zone entrainment, along-shore transport, and human health implications of pollution from tidal outlets. *J. Geophys. Res.*, *110*(C10025), doi:10.1029/2004JC002401.
Grimes, D. J., Feddersen, F., & Giddings, S. N. (2021). Long-distance/time surf-zone tracer evolution affected by inner-shelf tracer retention and recirculation. *J. Geophysical Research Oceans*. (revised)
Hally-Rosendahl, K., Feddersen, F., Clark, D. B., & Guza, R. T. (2015). Surfzone to inner-shelf exchange estimated from dye tracer balances. *Journal of Geophysical Research: Oceans*, n/a–n/a. doi: 10.1002/2015JC010844
Hally-Rosendahl, K., Feddersen, F., & Guza, R. T. (2014). Cross-shore tracer exchange between the surfzone and inner-shelf. *Journal of Geophysical Research: Oceans*, *119*(7), 4367–4388. doi: 10.1002/2013JC009722
Humphrey, C., Iversen, G., Skibiel, C., Sanderford, C., & Blackmon, J. (2019). Geochemistry of flood waters from the tar river, north carolina associated with hurricane matthew. *Resources*, *8*, 1–12. doi: 10.3390/resources8010048
Jamieson, R., Joy, D., Lee, H., Kostachuk, R., & Gordon, R. (2005). Transport and deposition of sediment-associated escherichia coli in natural streams. *Water Research*, *39*, 2665–2675. doi: https://doi.org/10.1016/j.watres.2005.04.040
Kastner, S. E., Horner-Devine, A. R., & Thomson, J. M. (2019). A conceptual model of a river plume in the surf zone. *Journal of Geophysical Research: Oceans*, *124*(11), 8060-8078. doi: https://doi.org/10.1029/2019JC015510
Kerpen, N., Schlurmann, T., Schendel, A., Gundlach, J., Marquard, D., & Hupgen, M. (2020). Wave-induced distribution of microplastics in the surf zone. *Frontiers in Marine Science*, *7*, 590565. doi: 10.3389/fmars.2020.590565
Kim, J., & Grant, S. (2004). Public mis-notification of coastal water quality: A probabilistic evaluation of posting errors at huntington beach, california. *Environmental Science and Technology*, *38*, 2497–2504. doi: https://doi.org/10.1021/es034382v
Kim, S. Y., Terrill, E. J., & Cornuelle, B. D. (2009). Assessing coastal plumes in a region of multiple discharges: The US-Mexico border. *Environmental Science & Technology*, *43*(19), 7450-7457. doi: 10.1021/es900775p
Kumar, N., & Feddersen, F. (2017). A new offshore transport mechanism for shoreline-released tracer induced by transient rip currents and stratification. *Geophysical Research Letters*, *44*(6), 2843–2851. (2017GL072611) doi: 10.1002/2017GL072611
Kumar, N., Voulgaris, G., Warner, J. C., & Olabarrieta, M. (2012). Implementation of the vortex force formalism in the coupled ocean-atmosphere-wave-sediment transport (COAWST) modeling system for inner shelf and surf zone applications. *Ocean Modelling*, *47*(0), 65 - 95. doi: 10.1016/j.ocemod.2012.01.003
Leecaster, M., & Weisberg, S. (2001). Effect of sampling frequency on shoreline microbiology assessments. *Marine Pollution Bulletin*, *42*, 1150–1154. doi: https://doi.org/10.1016/S0025-326X(01)00130-8
Lentz, S., Guza, R. T., Elgar, S., Feddersen, F., & Herbers, T. H. C. (1999, August). Momentum balances on the North Carolina inner shelf. *J. Geophys. Res.*, *104*, 18205-18240. doi: 10.1029/1999JC900101
Longuet-Higgins, M. S. (1970). Longshore currents generated by obliquely incident sea waves, parts 1 and 2. *J. Geophys. Res.*, *75*, 6778-6801.
MacVean, L., & Stacey, M. (2011). Estuarine dispersion from tidal trapping: a new analytical framework. *Estuaries and Coasts*, *34*, 45–59. doi: 10.1007/s12237-010-9298-x
Medellin, G., Torres-Freyermuth, A., Tomasicchio, G., Francone, A., Tereszkiewicz, P., Lusito, L., ... Lopez, J. (2021). Field and numerical study of resistance and

resilience on a sea breeze dominated beach in yucatan (mexico). *Water*, *10*, 1–21. doi: 10.3390/w10121806

Mei, C. (1989). *The applied dynamics of ocean waves.* World Scientific Publishing Co. Pte. Ltd.

Moulton, M., Chickadel, C., & Thompson, J. (2021). Warm and cool nearshore plumes connecting the surf zone to the inner shelf. *Geophysical Research Letters*, *48*, e2020GL091675. doi: https://doi.org/10.1029/2020GL091675

Moulton, M., Elgar, S., Raubenheimer, B., & Kumar, N. (2017). Rip currents and alongshore flows in single channels dredged in the surf zone. *Journal of Geophysical Research: Oceans*, *122*, 3799–3816. doi: 10.1002/2016JC012222

Neville, J., Emanuel, R., Nichols, E., & Vose, J. (2021). Extreme flooding and nitrogen dynamics of a blackwater river. *Water Resources Research*, *57*, e2020WR029106. doi: 10.1029/2020WR029106

Okubo, A. (1973). Effect of shoreline irregularities on streamwise dispersion in estuaries and other embayments. *Netherlands Journal of Sea Research*, *6*(1–2), 213–224. doi: 10.1007/s12237-010-9298-x

Rippy, M. A., Franks, P. J. S., Feddersen, F., Guza, R. T., & Moore, D. F. (2013). Physical dynamics controlling variability in nearshore fecal pollution: Fecal indicator bacteria as passive particles. *Mar. Poll. Bull.*, *66*, 151-157. doi: 10.1016/j.marpolbul.2012.09.030

Rippy, M. A., Stein, R., Sanders, B., Davis, K., McLaughlin, K., Skinner, J., ... Grant, S. (2014). Small drains, big problems: The impact of dry weather runoff on shoreline water quality at enclosed beaches. *Environmental Science and Technology*, *48*, 14168–14177. doi: https://doi.org/10.1021/es503139h

Rodriguez, A. R., Giddings, S. N., & Kumar, N. (2018). Impacts of nearshore wave-current interaction on transport and mixing of small-scale buoyant plumes. *Geophysical Research Letters*, *45*(16), 8379-8389. doi: 10.1029/2018GL078328

Roe, P. (1986). Characteristic-based schemes for the euler equations. *Annual review of fluid mechanics*, *18*, 337–365. doi: https://doi.org/10.1146/annurev.fl.18.010186.002005

Rogowski, P., Terrill, E., Schiff, K., & Kim, S. (2015). An assessment of the transport of southern california stormwater ocean discharges. *Marine Pollution Bulletin*, *90*, 135–142. doi: https://doi.org/10.1016/j.marpolbul.2014.11.004

Ruessink, B. G., Miles, J. R., Feddersen, F., Guza, R. T., & Elgar, S. (2001). Modeling the alongshore current on barred beaches. *J. Geophys. Res.*, *106*, 22,451-22,463.

San Diego County. (n. d.). *San diego beach information.* `http://www.sdbeachinfo.com/`. (Accessed: 2021-06-14)

Shchepetkin, A. F., & McWilliams, J. C. (2005). The regional oceanic modeling system (roms): a split-explicit, free-surface, topography-following-coordinate oceanic model. *Ocean Modelling*, *9*(4), 347 - 404.

Shuval, H. (2003). Estimating the global burden of thalassogenic diseases: human infectious diseases caused by wastewater pollution of the marine environment. *Journal of Water and Health*, *1*. doi: 10.2166/wh.2003.0007

Spydell, M. S., Feddersen, F., & Guza, R. T. (2009). Observations of drifter dispersion in the surfzone: The effect of sheared alongshore currents. *J. Geophys. Res.*, *114*(C07028). doi: 10.1029/2009JC005328

Spydell, M. S., Feddersen, F., Guza, R. T., & Schmidt, W. E. (2007). Observing surfzone dispersion with drifters. *J. Phys. Ocean.*, *27*, 2920-2939.

Steets, B., & Holden, P. (2003). A mechanistic model of runoff-associated fecal coliform fate and transport through a coastal lagoon. *Water Research*, *37*, 589–608. doi: https://doi.org/10.1016/S0043-1354(02)00312-3

Stidson, R., Gray, C., & McPhail, C. (2011). Development and use of modelling techniques for real-time bathing water quality predictions. *Water and the environ-*

ment, *26*, 7–18. doi: https://doi.org/10.1111/j.1747-6593.2011.00258.x

Suanda, S. H., & Feddersen, F. (2015). A self-similar scaling for cross-shelf exchange driven by transient rip currents. *Geophysical Research Letters*, *42*(13), 5427–5434. (2015GL063944) doi: 10.1002/2015GL063944

Taylor, G. (1953). Dispersion of soluble matter in solvent flowing slowly through a tube. *Proc. Roy. Soc. A*, *219*, 186-203.

Tennekes, H., & Lumley, J. L. (1972). *A first course in turbulence*. MIT Press.

Torres-Freyermuth, A., Medellin, G., & Salles, P. (2021). Human impact on the spatiotemporal evolution of beach resilience on the northwestern yucatan coast. *Frontiers in Marine Science*, *8*. doi: 10.3389/fmars.2021.637205

Tran, Y., Marchesiello, P., Almar, R., Ho, D., Nguyen, T., Thuan, D., & Barthelemy, E. (2021). Combined longshore and cross-shore modeling for low-energy embayed sandy beaches. *Journal of Marine Science and Engineering*, *9*, 979. doi: 10.3390/jmse9090979

U.S. Environmental Protection Agency, O. o. W. (2014). *National beach guidance criteria and required performance for grants* (No. EPA-823-B-14-001).

Warner, J. C., Armstrong, B., He, R., & Zambon, J. B. (2010). Development of a Coupled Ocean-Atmosphere-Wave-Sediment Transport (COAWST) Modeling System. *Ocean Modelling*, *35*, 230–244. doi: 10.1016/j.ocemod.2010.07.010

Willmott, C. (1981). On the validation of models. *Physical Geography*, *2*(2), 184-194. doi: https://doi.org/10.1080/02723646.1981.10642213

Wright, D., & Thompson, K. (1983). Time-averaged forms of the nonlinear stress law. *Journal of Physical Oceanography*, *13*, 341–346. doi: https://doi.org/10.1175/1520-0485(1983)013⟨0341:TAFOTN⟩2.0.CO;2

Wu, X., Feddersen, F., & Giddings, S. (2021a). Automated temporal tracking of coherently evolving density fronts in numerical models. *Journal of Atmospheric and Oceanic Technology*, *38*. doi: https://doi.org/10.1175/JTECH-D-21-0072.1

Wu, X., Feddersen, F., & Giddings, S. N. (2021b). Characteristics and dynamics of density fronts over the inner to mid-shelf under weak wind conditions. *Journal of Physical Oceanography*. doi: 10.1175/JPO-D-20-0162.1

Wu, X., Feddersen, F., & Giddings, S. N. (2021c). Diagnosing surfzone impacts on inner-shelf flow spatial variability using realistic model experiments with and without surface gravity waves. *Journal of Physical Oceanography*. doi: 10.1175/JPO-D-20-0324

Wu, X., Feddersen, F., Giddings, S. N., Kumar, N., & Gopalakrishnan, G. (2020, 06). Mechanisms of Mid- to Outer-Shelf Transport of Shoreline-Released Tracers. *Journal of Physical Oceanography*, *50*(7), 1813-1837. doi: 10.1175/JPO-D-19-0225.1

Young, I. (1999). *Wind generated ocean waves*. Elsevier.

Zimmer-Faust, A. G., Steele, J. A., Xiong, X., Staley, C., Griffith, M., Sadowsky, M. J., ... Griffith, J. F. (2021). A combined digital pcr and next generation dna-sequencing based approach for tracking nearshore pollutant dynamics along the southwest u.s/mexico border. *Front. Microbiol.*. doi: 10.3389/fmicb.2021.674214